catalysts

MDPI

Review

Perovskites in the Energy Grid and CO_2 Conversion: Current Context and Future Directions

Ahmad Tabish [1,2], Anish Mathai Varghese [1], Md A. Wahab [3] and Georgios N. Karanikolos [1,4,5,*]

1 Department of Chemical Engineering, Khalifa University, P.O. Box 127788, Abu Dhabi, UAE; tabishzhcet@gmail.com (A.T.); anish.varghese@ku.ac.ae (A.M.V.)
2 Global Innovative Center for Advanced Nanomaterials, School of Engineering, Faculty of Engineering and Built Environment, The University of Newcastle, Ring Rd, Callaghan 2308, Australia
3 Institute of Advanced Study, Chengdu University, Chengdu 610106, China; mabdul.wahab@outlook.com
4 Center for Catalysis and Separations (CeCaS), Khalifa University, P.O. Box 127788, Abu Dhabi, UAE
5 Research and Innovation Center on CO_2 and H_2 (RICH), Khalifa University, P.O. Box 127788, Abu Dhabi, UAE
* Correspondence: georgios.karanikolos@ku.ac.ae

Received: 28 November 2019; Accepted: 25 December 2019; Published: 9 January 2020

Abstract: CO_2 emissions from the consumption of fossil fuels are continuously increasing, thus impacting Earth's climate. In this context, intensive research efforts are being dedicated to develop materials that can effectively reduce CO_2 levels in the atmosphere and convert CO_2 into value-added chemicals and fuels, thus contributing to sustainable energy and meeting the increase in energy demand. The development of clean energy by conversion technologies is of high priority to circumvent these challenges. Among the various methods that include photoelectrochemical, high-temperature conversion, electrocatalytic, biocatalytic, and organocatalytic reactions, photocatalytic CO_2 reduction has received great attention because of its potential to efficiently reduce the level of CO_2 in the atmosphere by converting it into fuels and value-added chemicals. Among the reported CO_2 conversion catalysts, perovskite oxides catalyze redox reactions and exhibit high catalytic activity, stability, long charge diffusion lengths, compositional flexibility, and tunable band gap and band edge. This review focuses on recent advances and future prospects in the design and performance of perovskites for CO_2 conversion, particularly emphasizing on the structure of the catalysts, defect engineering and interface tuning at the nanoscale, and conversion technologies and rational approaches for enhancing CO_2 transformation to value-added chemicals and chemical feedstocks.

Keywords: carbon dioxide; reduction; conversion; perovskites; review; catalyst; redox reactions; chemical looping; artificial photosynthesis

1. Introduction

In the past decades, the increasing concentration of CO_2 in the atmosphere is attributed mainly to the utilization of fossil fuels and it has negatively impacted the climate [1–8]. The level of CO_2 in the atmosphere has increased from 322 ppm in 1967 to 407 ppm in 2017 and is predicted to reach to 600 ppm by 2100. Consequently, according to the International Panel for Climate Change (IPCC), the mean global temperature will increase by 1.9 °C by the year 2100. In 1992, many countries ratified the U.N. Framework Convention on Climate Change, which set out guidelines to reduce greenhouse gas levels in the atmosphere. In a comparative context, the average global emission of CO_2 due to the use of fossil fuels is in the order of 35 Gt, while the annual capture limit is 35 Mt. To help mitigate global warming, efficient technologies to reduce the levels of CO_2 and simultaneously produce value-added products,

such as chemicals and fuels, by its conversion are a sustainable solution [9–18]. To this extent, a number of approaches have been investigated for the conversion of CO_2 into fuels [19–28]. One example of such technologies is high-temperature conversion (HT), which dissociates CO_2 molecules into hydrocarbons at temperatures higher than approximately 2000 °C in vacuum [29]. The process is associated with high energy consumption, and has issues of instability of the converted molecules under the applied harsh conditions. Another technology is the solar thermochemical conversion (STC), which can produce hydrocarbons at temperatures higher than 1000 °C, and where the CO_2 conversion rate and selectivity, e.g., to CO, are often found to be better than that of the photocatalytic technologies. The operating temperature of this process is also high and thus the chemicals produced often face stability issues as well. Among the high-temperature methods, the reverse water–gas shift chemical looping is a lower temperature CO_2 conversion process with operating temperatures in the range of 500–700 °C [29]. In this process, the conversion of CO_2 into CO takes place followed by hydrogenation of CO into fuels via Fisher–Tropsch synthesis (FTS).

Recently, among various nanostructured materials, semiconductor-based photocatalysts have shown great potential for CO_2 conversion into chemicals such as H_2, CH_4, CH_3OH, and NH_3, via complex photoreactions that harness solar photons as energy sources [21–29]. This process in general needs a high energy input to activate CO_2. In order to yield chemicals and fuels, the chemistry and thermodynamics of CO_2 should be well-known, as conversion of CO_2 is thermodynamically unfavorable due to the fact that the bond energy of C=O is 750 kJ/mol, making it difficult to break down. To facilitate the cleavage of the C=O bonds, catalytic approaches, namely, photo [1,30], photochemical [2,31], electrochemical [32,33], and thermochemical [34,35] reactions, are mainly being investigated. For instance, the high energy required to break C=O bonds for the formation of C–H bonds toward photocatalytic reduction of CO_2 with H_2O into hydrocarbon products is provided by incident light. On the other hand, the thermochemical process involves high temperature and pressure, and it is often challenging to control reaction selectivity [1–3]. Pretreatment at different temperatures has been found to affect reactivity and selectivity, while the overall process is often complicated and challenging to control, making it difficult to convert CO_2 to the desirable products with high efficiency. To this extent, the development of CO_2 conversion technologies at low temperatures involving novel catalysts, such as perovskite-based ones, becomes more attractive than classical methods, due to the inherent advantages that these materials can offer, which include sustainable catalytic efficiency, tunable selectivity, potential for scaling up to industrial applications, and the ability to improve conversion efficiency and selectivity via optimizing the catalyst morphology and structure [19–29].

2. Perovskite Structures and Properties

Recently, there has been an increasing interest toward the exploration of perovskites in the field of energy and environment for applications such as fuel cells, CO_2 conversion, vehicle exhaust gas purification, and water gas reactions, because of their low price, tunable oxidation state, structural properties, and thermal stability [24,26,28,36–38], while fundamental investigation of these compounds has the potential to shed light on the relationship between catalytic activities and solid-state properties. Perovskites are often found with the general formula ABO_3, where A stands for the alkali metal (Li, Na, K, and so on) and/or alkaline-earth metal (Mg, Ca, Sr, Ba, and so on) or rare earth metal cation, occupying the 12-fold coordinated cube-octahedral cages of oxygen sublattice, and B indicates the transition metal cation (such as Mn, Co, Fe, Ni, Cu, or Ti), which is surrounded by six oxygen atoms in an octahedral coordination and is also responsible for catalytic activity and electron transfer [23,24,26,27,29]. According to the given formula, many important cations can fit into the A and B positions for making the final crystalline structure, to effectively tune the material properties and help improve conversion efficiency and selectivity. The metals in the perovskites' lattice are generally stable, as needed for the catalytic reactions at various conditions, while their cations in the A and B positions could be replaced as required via partial substitution [23,26,29].

Perovskite oxides mainly consist of a cubical crystalline structure where the cations have large ionic radii, which allow extensive coordination of oxygen molecules in the A-sites. Therefore, the larger A-site cations in the lattice (both in cubic and double-layered perovskites) are energetically favorable to be terminated at the AO surface. In fact, A-sites effectively block B-sites from coming into contact with reactants, such as CO_2, because less B-sites are exposed to the free surface to be available to participate in reactions, thus impacting the electrochemical transformations [26,27,29]. On the other hand, these cations have smaller ionic radii, thus less energy is utilized when they occupy the B-sites. When O and A join, cubic packs appear, while B occupies the octahedral voids of the packing. Thus, in an ideal compound structure, among the atom bonds, the B–O distance matches $a/2$ (where a is the unit cell length), while the A–O distance equals to a/ $\sqrt{2}$ [10]. The following equation summarizes the ionic radii relation: $(r_A + r_O) = (\sqrt{2}(r_B + r_O)$. Related studies have shown that the metal oxides are stable in their oxidative state and are thus used as catalysts in a variety of conditions with high efficiency and stability, while the ABO_3 structure and composition provide excellent tunability to control the final properties [10]. It has also been reported that the cubic form of perovskites is retained in the ABO_3 formula, although this structure is not always strictly obeyed, thus, for evaluation of the deviation from this structure, the tolerance factor (t) was introduced by Calio et al. [14]. Accordingly, a measure of the ionic distance of A and B can be provided as indicated in the following equation: $t = (r_A + r_O)/(\sqrt{2}(r_B + r_O)$. For an ideal perovskite, t suggests unity, while lower values can also be obtained ranging from 0.75 to 1.0, and in such instances, the cubical structure of the compound is distorted, forming tetragonal shapes, lower symmetries, and rhombohedral forms [14,26,27]. Notably, in perovskites whose t values exceed 1, hexagonal structures are observed. This observation results from the large ionic radii of A ions and the smaller B ions. An example of such a compound is $BaNiO_3$ perovskite, which possesses a hexagonal shape (Figure 1).

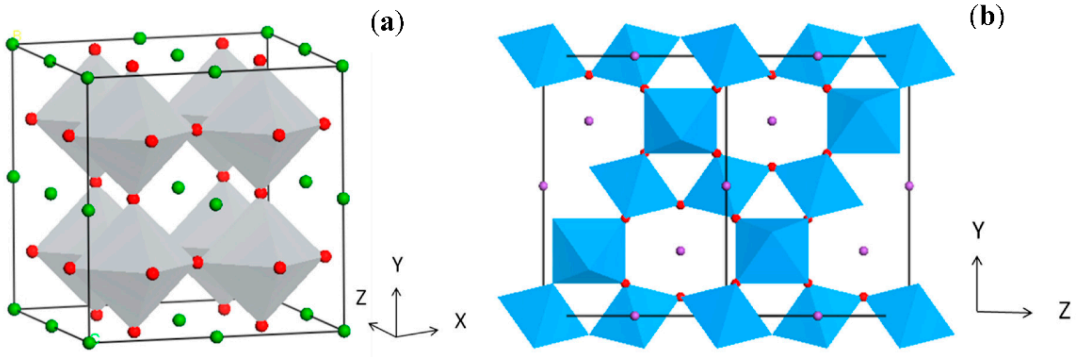

Figure 1. Perovskite crystal structure of (**a**) $BaNiO_3$ and (**b**) the double form of $Na_2Ta_2O_6$ (red, oxygen; green and purple, A-site cation; grey and blue, BO_6 octahedra) [38].

Research on perovskite-based systems for environmental and energy applications has intensified in the past two decades as energy demands increase and environmental constrains become more stringent [39]. To this extent, the use of nanostructured perovskites for producing hydrogen using water and solar energy, as well as conversion of CO_2 to generate hydrocarbons and value-added chemicals, is being intensively investigated [19,21–26]. Materials, such as those based on Ti, are being investigated for their photocatalytic performance. In the crystalline structure of these materials, the different tilting rates of octahedra usually produce various crystal forms, as well as optical and electronic properties. In particular, the tilting degree affects the band structure, photoluminescence, dielectric tendencies, hole transport, and electron properties [16,28,40,41]. The tuning ability of the perovskites provides significant benefits compared to binary oxides, since the A-sites and B-sites offer considerable opportunity for the alteration and design of the band structure and final properties. For the double perovskites (Figure 1), the stoichiometric presence of double cations on the B-sites is beneficial during photocatalysis by visible light. Combination effects, for example, with ferroelectricity, could benefit the photocatalytic activities, while these materials have the potential of offering a wide

range of overpotentials to introduce photoinduced reactions. When compared to metal oxides, these compounds have higher cathode conduction band (CB) energies, which are essential for the hydrogen evolution reaction (HER) [23,24,26–29,38].

High energy intake by incident light is needed to overcome reaction barriers and break the C=O bonds for the formation of C–H bonds in photocatalytic reduction of CO_2 into hydrocarbon products [2]. Progress towards commercialization is hindered by the availability of efficient, selective, and cost-effective catalysts. To this end, research efforts on the development of novel catalytic materials with tailored structural and morphological features for optimized performance, reactivity, selectivity, and stability are necessary [19,38,42,43]. The judicious choice of catalyst materials can tune CO_2 conversion reactions to achieve high selectivity and accelerated reaction rates. Among the available catalytic materials, perovskites are particularly attractive as mild operating conditions are used and wide control over the catalytic properties is achievable. Perovskites provide broad-spectrum activity, where applications can be anticipated utilizing visible and UV light, in particular, focusing on conversion into value-added chemicals for increasing chemical feedstocks and reducing CO_2 emissions in the atmosphere [1,2,5,38]. In this context, perovskite oxides have shown high stability, compositional flexibility, efficient catalytic capability, and long charge diffusion periods [23]. As a result, these materials can lead to accurate band gap and edge tuning, which are important in selective CO_2 reduction as well as in solar cell applications, due to their simple fabrication, high efficiency, and low costs [23,25,26,28,29,44,45]. Emerging CO_2 conversion technologies need to achieve reduction at a sustainable manner using mild operating temperatures, high conversion rates, and selectivity [46]. For example, earth-abundant and -derived perovskite materials are used in the gas–water shift reverse chemical looping to produce chemicals. The selection of technology is often based on manufacturing complexity, availability, productivity, and ability to tune the production of particular chemicals [47], as well as environmental assessment factors [48–56].

The structure of perovskite catalysts can play an important role in the conversion of CO_2 into value-added chemicals [19–21,23–26]. In particular, emphasis is given to achieve (i) high efficiency by enhancing mass transfer, (ii) the ability for separation of products, (iii) low-pressure drops, (iv) absence of clogging, (v) safety, and (vi) cost-and energy-effective production [36,57,58]. To this extent, the preparation method is important for controlling the properties and final structure of perovskites. Valuable information about tuning the material properties of perovskites can be extracted from their utilization in various applications including NO_x, oxidation of CO, combustion of hydrocarbons, and hydrogen production [58–60]. To affirm the application of these materials, their performance metrics have to be evaluated to determine the presence of active components [61–63]. For instance, much attention has been devoted to the development of structured perovskites that can be used in three-way converters. A challenge is testing the performance of the catalysts used [64–66]. In particular, the optimum operating conditions are difficult to determine, and therefore, the obtained results often deviate. Nevertheless, recent studies have shown significant improvement in the development of structured perovskite catalysts as demonstrated in Figure 2 [64]. Upon incorporation of metals to perovskites, the active phase constitutes a critical part of the structured form [67] contributing toward overcoming challenges related to catalytic performance, degradation, and diffusion limitations [19,42]. In particular, perovskite monoliths using various perovskite compositions, i.e., A = La, Ce, Y, Dy, or Sr; B = Mn, Cu, Fe, or Co, can be generated and tuned using steps such as extrusion of plastic pastes with catalytic powders, calcination, and drying procedures [64,65].

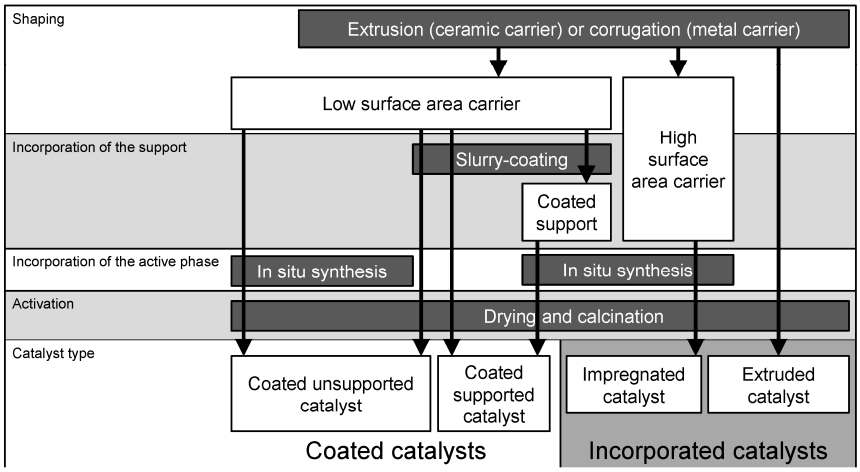

Figure 2. Preparation paths for structured perovskite catalysts [64].

3. Chemical Looping

CO_2 treatment systems combining conversion with capture in a cost-efficient manner are particularly attractive toward commercialization. On the capture side, reduction of the cost of CO_2 separation processes could be implemented by focusing on (i) improving the efficiency of the capture materials [6,7,68–70] and (ii) optimizing process design and reducing the cost of equipment [71–75]. In addition, considerable time and financial investments are needed in order to develop the relevant cost-effective technologies to enhance the production of chemicals, while reducing the associated costs of the used systems. In this regard, chemical looping is one of the promising technologies with the ability to separate CO_2 from fuel feeds, while it involves a high-energy combustion process that utilizes redox reactions. Figure 3 demonstrates the relation between cost reduction benefits vs. anticipated time to commercialization for various related technologies [74,76]. Evidently, reduction of the cost of separation can offer high potential for commercial CO_2 set-ups from capture to production of the value-added chemicals and energy.

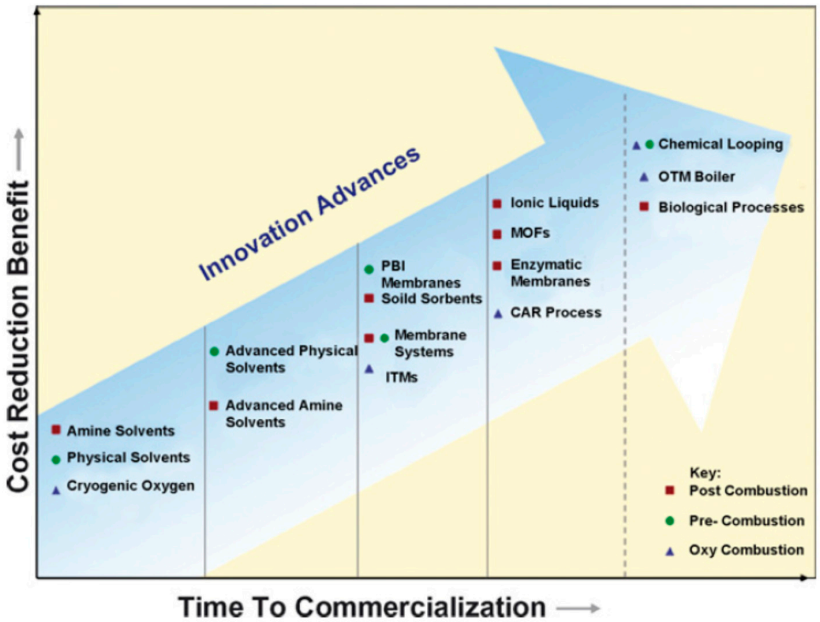

Figure 3. Cost reduction vs. time to commercialization for various CO_2 capture technologies. Adapted with permission from [74]. Copyright © 2008 Elsevier.

Studies have shown that chemical looping has evolved to accommodate various applications based on the recycle-based reaction design [51]. The process involves conversion, followed by regeneration of the involved solid materials [77]. According to Figure 4, significant developments on group A-1 process have been made. The process is split into two half-cycles. The reduction half-cycle reduces metal oxides, and the hydrocarbon fuels are oxidized to H_2O and CO_2 [78,79]. Fuels, such as biomass and coal, can be directly combusted in chemical looping via the oxygen uncoupling process [78–80]. A schematic representation of a mechanism for enhanced metal utilization in chemical looping reactions using reducible supports is also shown in Figure 5 [81].

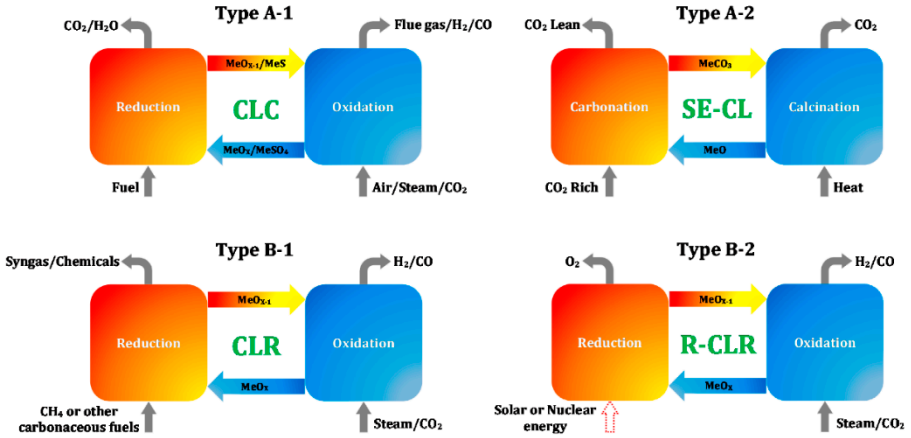

Figure 4. Chemical looping reactions. Top, CO_2 generation; bottom, production [79].

Despite the high cost and increased toxicity concerns, Ni-based structured perovskites have received great attention because of their enhanced catalytic activity [52,82]. For instance, an almost complete CH_4 conversion has been reported using chemical looping and Ni-based oxygen carriers. Though, results have shown that catalytic performance is often compromised due to partial oxidation and cycle repetitions [82]. Similarly, Ni-based structures are responsive to deactivation by coke deposition and sulfur poisoning. In this regard, material optimization is required to solve these issues. On the other hand, Fe-based components serve as reliable oxygen carriers because of their affordability, mechanical strength, and the fact that they are environmentally safe. They also tend to suffer less from sulfur and carbon depositions [83,84]. Significantly, these materials have high oxygen retention at various operating temperatures (600–1800 °C). As a result, most of the current chemical looping technologies perform dry reforming using Fe-based oxygen carriers.

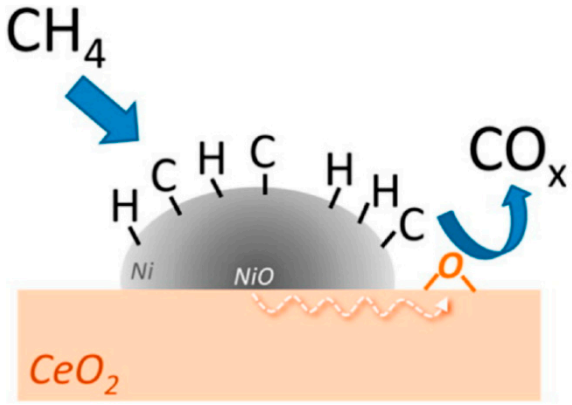

Figure 5. Schematic representation of the synergetic effect between reducible support and metal during chemical looping. Adapted with permission from [81]. Copyright © 2013 American Chemical Society.

4. Engineering of Oxygen Carriers

The shortcomings in industrial chemical looping require improvement of oxygen carriers. In particular, there are three critical pathways to consider: (i) standardization and activation of the oxygen carriers, (ii) introducing promoters, and (iii) mixing metal oxides to leverage multiple benefits [53,85]. Currently, significant attention is being devoted toward the improvement of Fe- and Ni-based oxygen carriers and notable improvements have been achieved on material structures, promoters, and the types of chemical looping processes in which these materials are used [86–88]. Both the support and promoters can be chemically and physically active, the latter creating physical barriers to enhance thermal stability and the former providing redox attributes to improve reactivity.

In the case of Ni-based oxygen carriers, various heat-resistant compounds (such as TiO_2, ZrO_2, and Al_2O_3) and spinels (such as $CaAl_2O_4$, $NiAl_2O_4$, and $MgAl_2O_4$) are considered as effective promoters. Among these oxides, NiO/Al_2O_3 demonstrates significant reactivity, strong resistance, and thermal stability, while preventing carbon formation upon chemical looping [89–91]. Ipsakis et al. [92] revealed metal–support interactions for the NiO/Al_2O_3 oxygen carrier, and a reduction reaction for the NiO/TiO_2 oxygen carrier. Tijani et al. [93] observed significant oxygen capacity for Ni-Co/ZrO_2, Ni-Cu/ZrO_2, and Ni-Fe/ZrO_2, along with minimal interaction with the Al_2O_3 support. A conversion rate of 37% was observed for Ni-Cu/ZrO_2 in the air reactor, with negligible effect in the fuel reactor. Park et al. [94] observed a strong influence of NiO type on the oxidation and reduction rates of Mg-incorporated NiO/Al_2O_3 oxygen carriers in conjunction to Mg content, and both the rates were observed to increase with reaction temperature as well as with gas concentration [94].

Inactive spinels, such as $NiAl_2O_4$, are formed due to the strong interaction between Al_2O_3 and NiO, thus resulting in partial loss of chemical activity. In this regard, studies have suggested that the chemical reaction should be supplied with excess Ni to retain sufficient content of the NiO oxygen carrier [95,96]. According to Chen et al. [97], superior performance in terms of plant efficiency was noted for the NiO oxygen carrier compared to CuO- and Fe_2O_3-based systems. On the other hand, chemical passivism can be deployed to enhance the inert form of the Al_2O_3 promoter [98,99]. Yu et al. [100] studied the effectiveness of the $NiAl_2O_4$ spinel for conversion applications. It was noticed that an enhanced catalytic performance, together with an anticoking benefit, was achieved by the contribution of improved textural properties of the catalyst. Beierlein et al. [101] investigated the structural influence of $NiAl_2O_3$ on the CO_2 methanation reaction. The yield was observed to be higher for the catalyst comprising high surface area Ni. A strong influence of spatial distribution of Ni as well as support stability was also reflected on catalyst stability. In another study, Baek et al. [102] reported an accelerated rate of oxygen transport for Mg-Al layered double hydroxide-supported NiO oxygen carriers compared to Al_2O_3- or MgO-supported versions, on account of enhanced physicochemical features.

The addition of MgO/CaO when preparing Al_2O_3/NiO oxygen carriers has led to the creation of stable spinels. The use of reducible oxides, such as CeO_2, also increased the potential of Ni-based compounds as oxygen carriers, while additional important properties are realized due to the synergetic effects of CeO_2 and Ni [103–106]. After the reduction cycle, Ni particles are composed of two main phases, i.e., the metallic form and NiO. CH_4 is decomposed on the metallic surface of Ni forming a carbonaceous species, which is then gasified using oxygen from CeO_2 [106]. During this process, the lost oxygen is replenished at the core of Ni particles. Therefore, a continuous reduction is assured for the Ni particles. Even though Ni/CeO_2 oxygen carriers provide a high reactivity to CH_4, the high utilization and exposure to carbon formation reduce the surface area during chemical looping. CeO_2 sintering becomes more dominant after repeated cycles, an issue that needs to be fixed before realization in industrial applications [107–109]. Hossain et al. [110] reported a considerable reduction in nickel aluminate generation for NiO/Ce-doped Al_2O_3 oxygen carrier through the reduced interaction between metal and support. Notably, the availability of approximately 70% of incorporated NiO to proceed with reduction reactions was evidenced. The cyclic stability was also evidenced from the repeated redox reactions. Zhao et al. [111] investigated the effectiveness of Ni/Mg/$Ce_{0.6}Zr_{0.4}O_2$/Al_2O_3 for CO_2

conversion applications. CO_2 conversion rates of 4% and 61% were observed at 1 and 6 bar, respectively, and at 860 °C.

Fe-based oxygen carriers have also attracted considerable attention in chemical looping applications [112,113]. Bhui et al. [114] investigated the chemical looping process supported by Fe_2O_3 oxygen carriers. Interestingly, a significantly improved CO_2 yield of 88.7% was discerned, though only 17.5% was observed in the absence of Fe_2O_3. Hu et al. [115] developed an oxygen carrier based on Fe_2O_3/Al_2O_3 exhibiting superior crystal cell shrink resistance and significantly enhanced specific surface area. As a result, an increase of 13% and 37% in reduction and oxidation rates, respectively, was noticed, along with an appreciable regenerability after five redox cycles. In another study, Diego et al. [116] reported the effects of Fe content and elevated temperature in achieving effective chemical looping for Fe-Al oxygen carriers. Further studies have shown that promoters, such as MgO, Al_2O_3 and TiO_2, easily induce solid-to-solid transformations with the Fe oxides during continuous cycling. Thus, based on the promoter being used, compounds such as $MgFeO_4$, $FeTiO_3$, $Ca_2Fe_2O_4$, Fe_2SiO_4, and $AlFeO_4$ can be formed. These compounds are mainly formed during redox reactions, where the metal ferrites become physical barriers. Therefore, they prevent iron oxide sintering, while the oxygen-carrying capacity reduces since the ferrites are strong reducing agents [117,118]. In that regard, their oxygen storage capacity reduces considerably and it becomes difficult for the unreactive compounds to decompose. Significantly, considering that the spinel compounds are formed easily, the addition of the right amounts of Mg to the chemical looping reaction can stop the formation of $FeAl_2O_4$ [119]. On the other hand, $MgAl_2O_4$ contributes also through its high chemical and thermal stability, and specific heat capacity. Hafizi et al. [120] compared the performance of Fe_2O_3/Al_2O_3 and $Fe_2O_3/MgAl_2O_4$ oxygen carriers. It was observed that Mg modification of alumina could improve the performance of the oxygen carrier in chemical looping and sorption-enhanced chemical looping reforming processes. This was attributed to the prevention of $FeAl_2O_4$ spinel generation and resultant improvement in the activity of oxygen carrier under the influence of Mg by the generation of $MgAl_2O_4$. Liu et al. [121] observed an appreciable performance for an oxygen carrier based on Fe_2O_3/TiO_2 during 30 redox cycles. The combined incorporation of La and Ce was favorable to improve sintering as well as carbon deposit resistance of Fe_2O_3/Al_2O_3, as demonstrated by the work of Tang et al. [122]. An Fe_2O_3/ZrO_2-ZrO_2 core-shell structured oxygen carrier with enhanced performance in redox activity, sintering resistance, and structural as well as thermal stability was developed by Hu et al. [123] for CO_2 conversion applications.

Perez-Vega et al. [124] developed an oxygen carrier using $MnFe_2O_3$, which was efficient in terms of reactivity and mechanical properties. Furthermore, the addition of kaolin during the calcination step was beneficial to enhance the reactivity and strength, yet at the expanse of oxygen transport capacity. The applicability of TiO_2-doped $MnFeO_3$ was studied as well. Enhanced oxygen uncoupling as well as magnetic features for this oxygen carrier under the conditions of both oxidation and reduction were evidenced [125].

CeO_2 promotes iron oxides in chemical looping because of its high reactivity to methane using lattice oxygen [126]. Redox reactions facilitate the transfer of oxygen and its release from the lattice. When Ce^{4+} ions are replaced by cations of lower valence, space for oxygen is created at the active sites. After the consumption of surface oxygen, the additional gas is transferred to the surface [127]. In that regard, the presence of CeO_2 increases the reduction of Fe_2O_3. The effectiveness of Fe_2O_3-CeO_2/Al_2O_3 oxygen carrier was studied by Kang et al. [128], and a significant redox activity was evidenced. Also, the generation of syngas with high purity was achieved, together with a molar ratio of 2 for H_2/CO. Hafizi et al. [129] reported sustainable activity for $Fe/Ca/Al_2O_3$ oxygen carrier upon 15 cycles of oxidation and reduction.

The applicability of the $NiFeAlO_4$ spinel as a self-sustained oxygen carrier has been investigated by Kuo et al. [130] for the conversion of CO_2 to H_2. A significantly enhanced agglomeration resistance was observed for this oxygen carrier in comparison to other studied systems, such as NiO, Fe_2O_3, and $NiFe_2O_4$. Notably, the reduction reaction in a fixed bed reactor confirmed enhanced H_2 generation

and CO_2 conversion. Zaabout et al. [131] made a performance comparison for $(FeNiAl)_3O_4$ with Fe_2O_3, and observed that the $(FeNiAl)_3O_4$ spinel was more efficient with respect to conversion rate and cyclic stability. In another work, Hu et al. [132] reported the use of the $NiO/Fe_2O_3/MgAl_2O_4$ oxygen carrier for CO_2 conversion via the chemical looping process. Under the conditions of reduction capacity >2 and temperature >873 K, a high extent of Fe_2O_3 reduction was discerned. Regarding the cyclic operations, superior stability was attained for five cycles.

Some attempts using Cu-based oxygen carrier systems have also been made. Huang et al. [133] introduced CuO/Al_2O_3 oxygen carrier exhibiting superior carbon deposition and deactivation resistance for multicycle redox operations, on account of better distribution of CuO on Al_2O_3. Furthermore, an oxygen carrier consisting of CuO, Fe_2O_3, and $MgAl_2O_4$ has been explored for chemical looping combustion applications [134]. Adanez-Rubio et al. [135] discussed the applicability of CuO/Mn_3O_4 as an oxygen carrier for chemical looping. The lifetime of this oxygen carrier was found to be significant for a large oxygen carrier/fuel ratio.

An oxygen carrier based on hierarchical Co/MgO rich in oxygen sites, activity, thermal reliability, and Co dispersion was reported by Li et al. [136]. Moldenhauer et al. [137] developed the $CaMnO_3$ oxygen carrier with high potential of cost-effectiveness. In addition, this oxygen carrier had the capability to enable reactivity through effective release of oxygen to the gaseous state, together with superior attrition resistance. Sulfur poisoning was a drawback of this material. Zhu et al. [138] found that Ce doping was more effective to enhance the reactivity, multicycle stability, syngas yield, and CO_2 activation of hexaaluminate oxygen carriers in comparison to doping with other metals, such as Fe, Si, and Zr. In another study, Huang et al. [139] reported appreciable stability for Fe-doped hexaaluminate oxygen carriers after 50 redox cycles.

5. CO_2-Derived Fuels

The conditions of the available CO_2 sources upon capture play an important role in the subsequent separation and conversion technology. In the post-combustion process, gases are obtained when fossil fuels burn where the composition of CO_2 is 3%–20%. In pre-combustion, higher CO_2 levels are typically obtained, reaching 15%–40% at higher temperatures. A shift reaction occurs during the production of synthesis gas using a water–gas combination, where fuel oxy-combustion is established [140].

5.1. Electrolysis

CO_2 can be reduced electrolytically into fuels in analogy to water electrolysis, where oxygen forms at the anode, while the reduction of the gas occurs at the cathode [141]. In this case, the electrolytic process is dependent on the catalyst used in the reaction and can yield products that include methanol, formic acid, ethylene, formaldehyde, and methane. Challenges such as catalyst deactivation, high overpotentials in cells, and limited current densities need to be overcome. Given that the thermodynamic potential of CO_2 is analogous to that of splitting water, the reduction of the gas results in a low faradaic efficiency [142]. Copper, for instance, reduces CO_2 having substantial current densities, workable faradaic efficiency, and cell overpotentials. As a result, hydrocarbons such as ethylene and methane are formed.

Sathre et al. [143] examined CO_2 reduction at high temperatures using solid oxide electrolytic cells (SOEC). The feasibility of reduction at high temperatures is to lower the electrical charge required, while increasing the rate of the electrode reaction [144]. In this case, efficient reduction of CO_2 can occur at approximately 800 °C using perovskites, such as $La_{0.8}Sr_{0.2}Cr_{0.5}Mn_{0.5}O_3$ (LSCM), to accelerate electrode kinetics. Pb-ceria composites are also used in the reduction reaction as co-catalysts [144,145]. Interestingly, at high temperatures, the co-electrolysis of water and CO_2 leads to the production of synthetic gas and oxygen at the cathode and anode, respectively. This process can operate with an efficiency of up to 70% [146].

5.2. Thermochemical and Photoelectrochemical Conversions

Thermochemical and photoelectrochemical conversions have received rather less attention compared to SOEC because they are still at an earlier research stage, thus there is still a long way to go to reach large-scale applications [147]. Similar to water splitting, the main challenge of the photochemical approach is the development of suitable photocathodes to facilitate the reduction process [148]. The issue of CO_2 availability in aqueous form also exists because of poor solubility. Nevertheless, investigations focus on non-aqueous solvents and three-phase interfaces (solid/liquid/gas) [149]. In this arrangement, the metallic electrodes should be partially dipped in CO_2 solutions, while the gas is supplied in the vapor stage.

On the other hand, thermochemical reduction is also under investigation using metal oxides [150,151]. For instance, at 1600 °C, ZnO is reduced to Zn using solar energy. Subsequently, at 360 °C, Zn is oxidized by CO_2 forming ZnO and CO. Although the thermochemical approach is viable for the conversion of CO_2 into value-added chemicals, it can be enhanced through the co-reaction between H_2O and CO_2, e.g., using CeO_2, to produce O_2, CO, and H_2 [152]. This reaction starts with the reduction of CeO_2 at temperatures of approximately 1420–1640 °C. Then oxidation using CO_2 and H_2O follows at approximately 900 °C. While the predicted solar-to-fuel conversion ranges between 16%–19%, only about 8% is realized experimentally [153]. Heat loss is also a significant issue in the reaction. Solar-assisted conversion using hydrogen is also under investigation [154]. For instance, synthetic gas is made by the reaction of hydrogen and CO, while the hydrogenation of CO_2 creates other fuels that are easy to distribute, store, and use.

6. Photon Capture

The formation of solar fuels starts with the identification and development of the proper materials for photon capture [154,155]. Suitable materials as solar absorbers used in electrochemical reactions include oxynitrides, carbon, nitrides, oxides, and carbon nitrides [156,157]. For photoelectrochemical fuel production, the absorbers should have the proper band gap and structure to use most of the available solar radiation, while they should also exhibit sufficient charge transport efficiency and stability. Furthermore, the optimum materials should be non-toxic, inexpensive, and abundant. In one case, metal deposition was conducted on thin print spots to target n-type porous Fe-based binary oxides and p-type Bi-based semiconductors. It was determined that $FeVO_4$ and $CuBi_2O_4$ were suitable visible-light semiconductors, while Bi-Cu and Bi-Ag-Cu composite systems also showed significant photocurrent capabilities.

Further assessments of suitable materials for water splitting have evaluated sulfides, fluorides, metal oxides, and their combinations. MnV_2O_6, in particular, has been experimentally proven to bear desirable water splitting properties [158–160]. Recent evidence also suggests that organometal halide perovskites have the potential of being efficient photo-absorbers, while they are formed from naturally occurring materials. As research continues with the development of suitable photo-absorbers and investigation of their structure–property relationships, an additional challenge that needs to be addressed is the stability under photoelectrochemical conditions.

7. Artificial Photosynthesis

In recent years, the production of solar fuels using artificial photosynthesis is under intense investigation, where CO_2 is reduced and the energy produced is stored in a chemical form [161]. The objective has been the scalable production of systems that can reduce CO_2 using water and solar energy to generate electrons [162]. To this end, ZnO/ZnTe/CdTe triple-layered gold-plated core photocathode and a perovskite solar cell containing $CH_3NH_3PbI_3$ have been employed. It was determined that light harvesting achieves high energy photons (>2.14 eV) at the photocathode. The utilization of perovskite halides in photovoltaic processes has attracted attention because these materials are abundant, have high climbing efficiencies, and have a relatively low cost of synthesis.

Photochemical CO_2 conversion to value-added chemicals is realized using homogeneous and heterogeneous systems, where CO_2 is reduced at photovoltaic junctions [163]. In that regard, thermodynamics forms the fundamentals of reduction using photovoltaic cells. The challenge in such utilization of photovoltaics is the development of abundant earth materials, which will also be non-toxic and affordable, and they will constitute sunlight-stable photovoltaic compounds [163–165]. In a prototype based on an imidazolium salt derivative developed by Toshiba, the conversion of CO_2 to ethylene glycol was realized at high efficiency and without harmful byproducts [164]. In this regard, molecular interactions between the catalysts coated on a metal surface, where CO_2 molecules are reduced, played a dominant role in the efficiency. Most of the currently available photomolecular technologies use two-electron reduction-conversion processes. Toshiba's new molecular catalysts, however, employ multiple conversion where ethylene glycol is produced during reduction. It was determined that the efficiency of the catalysts can reach up to 80% [23]. Toshiba is further investigating the development of molecular catalysts to improve their application in artificial photosynthesis.

Extensive studies are being conducted on polar materials to understand their potential as semiconductors to be used in photovoltaic applications [165,166]. In particular, the movement of dipoles in these materials is activated by sunlight, and as a result, charge carriers are generated. These materials comprise ferroelectrics, which are determined to exhibit pyro- and piezo-electricity. Research on these materials was enhanced with the discovery of photocurrent generation using para-electric $BaTiO_3$. The detection of the band gap in cadmium telluride including zinc sulfide was also a contributing factor. Nevertheless, most of the research has concentrated on the photovoltaic effect in non-centrosymmetric crystals, also called the galvanic effect [167]. The ferroelectric phenomena refer to the production of steady streams of current in short circuits.

The initial model for the bulk photoelectric effect utilized asymmetric materials; however, recent developments have seen the adaptation of theories on shift currents [168]. To this end, the photoelectric concept could be explained from a microscopic perspective using the shift and ballistic mechanism models. Firstly, the ballistic model for anisotropic and isotropic materials is centrosymmetric utilizing the *p*–*n* junctions in solar cells [169]. The model projects itself when the photoelectric materials are exposed to sufficient thermal illumination after which the valence bands get excited. As a result, a photocurrent is generated through the conduction band. During this process, the carriers lose energy and therefore move to the conduction band's bottom via band-to-band transitions. This movement is meant to create equilibrium and thus continue the production of the bulk photocurrent [170]. Notably, the current shift model is characterized by a quantum mechanical nature, which implies that coherent excitations cause the thermal carriers.

Considering hydrogen production, artificial photosynthesis provides the means for efficiently converting solar energy to hydrogen [171,172]. To this end, powered water electrolysis using photovoltaics is a promising approach, yet the technique often suffers from low solar-to-fuel conversion efficiencies. Solar thermochemical conversion, on the other hand, offers a relatively high theoretical efficiency and can support large-scale production due to utilization of the vast solar spectrum.

To this extent, versatility in the preparation of various perovskite configurations is important. For example, useful information can be extracted from the development of perovskites based on metal halides, which have gained attention for the production of solar cells [173]. These materials have high potential, for instance, emitting bright light in diodes with considerable efficiency, having therefore the capability to impact the electronics industry, where both inorganic and organic materials can be combined to a composite [174,175]. The high conduction ability of perovskites can also be leveraged and used in making polycrystalline films. The ability to efficiently fabricate such structures can allow the implementation of solution-processing techniques to create high-performance systems [174]. Yet, most of the methods used cannot be easily consolidated for large-scale production [24]. Recent studies have explored vapor-based methods deeming them as technologies that can be adopted in the semiconductor and coatings industry for large-scale implementation.

8. Solar Fuels

Developments in green electricity production and electric transportation can play a vital role in reducing the emission levels of greenhouse gases [176]. It is projected that by 2050, the levels of greenhouse emissions will be reduced by approximately 80% following the adoption of alternative fuels. Indicatively, the White House aims to promote clean energy to drastically cut greenhouse gas pollution by 2035 [177]. Therefore, given the fact that the global consumption of electricity is being increased, and taking into account the lack of efficient means of storage, the development of alternative energy is imperative and important in order to ensure sustainability. In addition, more energy is required to propel industries, such as manufacturing and transportation, within the continuous digitalization transformation [178]. Solar energy is classified as a carbon-free source and it has the highest potential in replacing the consumption of fossil fuels. Various challenges have to be resolved to utilize it competitively. Firstly, ample energy storage solutions should be developed considering the intermittent nature of the resource. Secondly, plans on how to achieve the production of solar energy at a large scale to be used in transportation and other sectors should be identified. Solar energy currently accounts for a small fraction of the energy supply to grid systems [179–181]. Unfortunately, a setback is its intermittent supply. Production, however, can be supplemented by wind in places with less sunlight. According to the USA Energy Information Administration, it is expected that the production of solar energy will increase by 5%–7% yearly [182–184]. Yet, a challenge is to develop, in parallel, efficient energy storage systems. Most importantly, such systems should be carbon-neutral and robust to allow grid stability under the future demands [185]. Indicatively, if a 75% efficiency of electrolytic cells is merged with that of a cycle steam and a gas turbine generator using hydrogen at 60%, the result would be 45% efficiency [186,187]. Yet, the storage capacity for hydrogen and batteries cells should be considerably optimized.

Hydrocarbons, on the other hand, have high energy densities and can be synthesized from CO_2 (Figure 6) [188]. Natural gas synthesis can be feasible on a large scale using CO_2 and hydrogen with an efficiency in the order of 80%. The product can have an energy density that is three times higher that of the naturally occurring product. Therefore, considering the pivotal role of chemical fuels in electricity generation, solar energy conversion can be leveraged to create a desirable distribution [189,190]. Synthetic gas can be stored and supplied to the consumers to power heating and vehicle systems. Indicatively, in Germany, the storage capacity of natural gas exceeds 200 TWh. The country can supply this amount for several months. In addition, with the production of synthetic gas, the applications of the resource could extend, for instance, in fertilizer production, transportation, and pharmaceuticals [188,191,192].

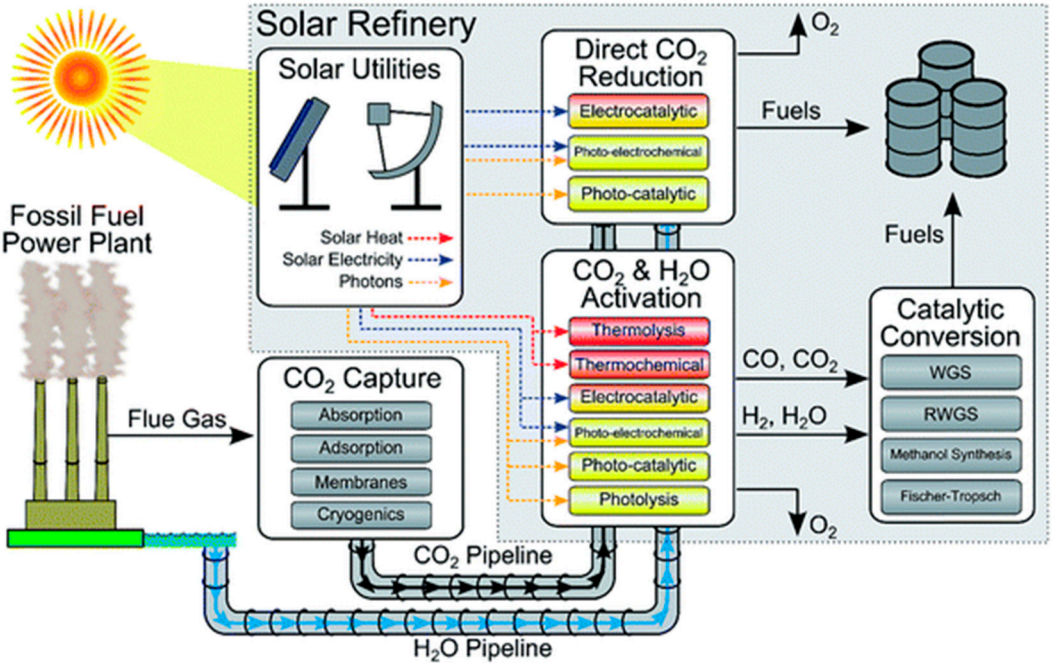

Figure 6. Solar refinery scheme. Adapted with permission from [188]. Copyright © 2015 The Royal Society of Chemistry.

Over the years, experts have tested the potential of solar fuels in the production of clean energy. Hydrogen, as an elemental fuel, has desirable attributes necessary for the production of clean energy; yet, it lacks a high volumetric density, and as a result, it cannot be easily stored or distributed [140,193–196]. On the other side, conversion of CO_2 to CH_4 attracts significant attention, while the reaction between CO_2 and H_2 also produces fuel that is easy to distribute, store, and use in existing supply infrastructures (Figure 6) [188]. On that note, the concept of converting CO_2 using solar energy is viable, thus generating solar fuels from green sources exhibiting sufficient energy densities [107]. Photocatalytic and photothermal applications have the potential of achieving considerable energy conversion efficiencies and commercial viability [140]. At present, the contribution of artificially generated solar fuels remains small, while efforts on reducing production costs need to be intensified, while challenges in the CO_2 capture and sourcing front as well as in enhancing the efficiency of solar-assisted conversion of CO_2 should be considered. The objective is to reduce production costs, extend the lifetime of the systems, and invest in infrastructural developments. These efforts will help bridge the gap between deployable technologies and current laboratory work.

Table 1 summarizes literature that reported perovskite catalysts for solar thermochemical CO_2 conversion applications. Sr doping is a suitable method to enrich the CO yield of the $LaMnO_{3-\delta}$ perovskite catalyst as highlighted by the work of Yamazaki et al. [197]. Demont et al. [198] indicated a two-step cycling for the redox activity of non-stoichiometric $La_{1-x}Sr_xMnO_{3-\delta}$ upon solar-to-fuel conversion of CO_2. Nair et al. [199] supported the superior CO production efficiency of $La_xSr_{1-x}MnO_3$ perovskite catalysts, along with interesting reliability, by pointing out the benefit of Mn influence. An appreciable CO yield of 133.9 µmol/g was observed for the $La_{0.5}Sr_{0.5}MnO_3$ perovskite at 1673 K, as suggested by the study of Dey et al. [200]. At the same time, 1.8-fold higher CO yield was achieved by the $Y_{0.5}Sr_{0.5}MnO_3$ perovskite compared to $La_{0.5}Sr_{0.5}MnO_3$.

Upon CO_2 splitting, Nair et al. [201] observed superior reactivity for the $La_xSr_{1-x}MnO_3$ perovskite prepared using the Pechini approach in comparison to solid-state, glucose-assisted, and glycine combustion approaches. Riaz et al. [202] developed a lanthanum strontium manganite perovskite-based catalyst using electrospinning. Improved redox kinetics for this catalyst, together with an appreciable CO yield of 854.20 µmol/g per redox cycle consisting of reduction at 1400 °C and oxidation at 1000 °C, was reported. Furthermore, the electrospun catalyst was rich in structural stability.

Carrillo et al. [203] reported the effectiveness of Cr infusion to significantly enhance CO production kinetics using the $La_{0.6}Sr_{0.4}MnO_3$ perovskite. Likewise, good cyclic stability was offered through the prevention of structural decay. Bork et al. [204] also pointed out enhanced efficiency and fuel yield of the $La_{0.6}Sr_{0.4}Mn_{0.2}Cr_{0.8}O_{3-\delta}$ perovskite catalyst for solar-to-fuel applications. Luciani et al. [205] highlighted the possibility of Fe infusion to boost the redox characteristics of the $La_{0.6}Sr_{0.4}MnO_3$ perovskite. Although, the CO yield was observed to reduce with Fe content. Ezbiri et al. [206] reported significant redox activity for an Al-doped form of the $La_{1-x}Sr_xMn_{1-y}Al_yO_{3-\delta}$ perovskite catalyst.

Cooper et al. [207] revealed the feasibility of Ca or Sr (A-site) as well as Al (B-site) doping to significantly improve the reduction rate of lanthanum manganite perovskite catalysts. Compared to reference CeO_2, values up to 13 times higher were achieved for these doped lanthanum manganite perovskite forms, i.e., $La_{0.6}Sr_{0.4}Mn_{0.6}Al_{0.4}O_3$ and $La_{0.6}Ca_{0.4}Mn_{0.6}Al_{0.4}O_3$. Sastre et al. [208] reported great redox properties with acceptable cyclic performance for $La_{0.6}Sr_{0.4}Mn_{1-x}Al_xO_3$ perovskite. The extent of reduction was increased with Al content, while the oxidation extent was found optimal at a content of $Al_x = Al_{0.5}$.

Bork et al. [209] observed an almost 25-fold higher CO_2 splitting ability for the $La_{0.6}Sr_{0.4}Cr_{1-x}Co_xO_{3-\delta}$ perovskite compared to ceria. By the use of this catalyst, the added benefit of reduced solar-to-fuel reactor temperature of approximately 300 °C was reported. This catalyst also demonstrated good cyclic performance. Hare et al. [210] revealed the effectiveness of silica support to enhance CO production of the $La_{0.75}Sr_{0.25}FeO_3$ perovskite catalyst. Accordingly, an improvement of approximately 200% was observed at a relatively low temperature. This was attributed to silica-promoted surface area increase of the perovskite [211].

Hare et al. [212] prepared a $La_xCa_{1-x}Fe_yMn_{1-y}O_3$ perovskite catalyst and disclosed that the combinational influence of Ca and Fe could enrich structural stability. Ramos et al. [213] examined the role of B-site transition metals, such as Co, Fe, and Mn, in $LaCo_xFe_yMn_{1-x-y}O_3$ for low temperature solar-to-CO conversion. The surface segregation of Co and Fe contributed to the activity of this catalyst.

Dey et al. [214] reported enhanced CO production for a catalyst based on $Y_{0.5}Sr_{0.5}MnO_3$ at comparatively low redox temperature conditions on account of highly disordered/distorted structural influence. Rao and Dey [215] acquired a CO yield of 757 µmol/g at 1173 K by the use of the $Y_{0.5}Sr_{0.5}MnO_3$ perovskite. At 1673 K, an O_2 release of 483 µmol/g was observed for this catalyst. Takalkar et al. [216] reported the beneficial effect of reduced Pr, as well as increased Sr content, to enhance the O_2 release extent and CO yield of the $Pr_xSr_{(1-x)}MnO_{3-\delta}$ perovskite catalyst for solar-to-fuel conversion of CO_2. Compared to CeO_2, a considerably higher CO generation efficiency was reported for the $Pr_{0.5}Sr_{0.5}MnO_{3-\delta}$ perovskite material [217].

Table 1. Perovskite catalysts in solar thermochemical CO_2 conversion.

Catalyst	Reactor	Reduction Temperature (°C)	Reducing Atmosphere	Oxidizing Atmosphere	CO Yield (μmol/g)	O_2 Yield (μmol/g)	Reference
$LaMn_{0.5}Co_{0.5}O_3$	TGA	1400	<2 ppm O_2 premixed Ar	50% CO_2/Ar	145	83	Nair et al. [199]
$Ba_{0.5}Sr_{0.5}FeO_3$	TGA	1000	<2 ppm O_2 premixed Ar	50% CO_2/Ar	136	582	Nair et al. [199]
$La_{0.5}Sr_{0.5}MnO_3$	TGA	1400	<2 ppm O_2 premixed Ar	50% CO_2/Ar	269	248	Nair et al. [199]
$La_{0.5}Sr_{0.5}MnO_3$	TGA	1500	10 ppm O_2 premixed N_2	1 atm CO_2	230	111.6	Dey et al. [200]
$Y_{0.5}Sr_{0.5}MnO_3$	TGA	1400	10 ppm O_2 premixed N_2	1 atm CO_2	196.4	108	Dey et al. [200]
$La_{0.6}Sr_{0.4}Mn_{0.6}Al_{0.4}O_3$	TGA	1400	<2 ppm O_2 premixed Ar	50% CO_2/Ar	205	210	Nair et al. [201]
$La_{0.25}Sr_{0.75}MnO_3$	TGA	1400	N_2	CO_2/air	786.32 ± 41.6	516.24 ± 19.55	Riaz et al. [202]
$La_{0.6}Sr_{0.4}Cr_{0.75}Mn_{0.25}O_3$	TGA	1400	Ar	0.5 atm CO_2	~7 *	~1.2 *	Carrillo et al. [203]
$La_{0.6}Sr_{0.4}MnO_3$	TGA	1350	N_2	CO_2	469.1	348.8	Luciani et al. [205]
$La_{0.6}Sr_{0.4}Mn_{0.8}Fe_{0.2}O_3$	TGA	1350	N_2	CO_2	329.9	286.0	Luciani et al. [205]
$La_{0.6}Ca_{0.4}Mn_{0.6}Al_{0.4}O_3$	TGA	1375	3×10^{-5} bar O_2 mixed Ar	50% CO_2/Ar	ca. 420	-	Cooper et al. [207]
$La_{0.6}r_{0.4}Mn_{0.6}Al_{0.4}O_3$	Fixed bed reactor	1250	Ar	5% CO_2/He	114	266	Sastre et al. [208]
$La_{0.6}Sr_{0.4}Cr_{0.8}Co_{0.2}O_{3-\delta}$	TGA	1200	Ar	50% CO_2/Ar	157	-	Bork et al. [209]
SiO_2-supported $La_{0.75}Sr_{0.25}FeO_3$	Quartz microreactor connected with Cirrus MKS MS	950	10% H_2/He	10% CO_2/He	1700	-	Hare et al. [211]
$La_{0.75}Ca_{0.25}MnO_3$	Quartz microreactor connected with Cirrus MKS MS	950	10% H_2/He	10% CO_2/He	1680	-	Hare et al. [212]
$La_{0.5}Ca_{0.5}Fe_{0.25}Mn_{0.75}O_3$	Quartz microreactor connected with Cirrus MKS MS	600	10% H_2/He	10% CO_2/He	1450	-	Hare et al. [212]
$LaCo_{0.5}Fe_{0.25}Mn_{0.25}O_3$	Quartz U-tube reactor connected with Cirrus MKS MS	550	10% H_2/He	10% CO_2/He	1780	-	Ramos et al. [213]
$Y_{0.5}Sr_{0.5}MnO_3$	TGA	1400	Ar	40% CO_2/Ar	757	483	Dey et al. [214]
$Y_{0.5}Ca_{0.5}MnO_3$	TGA	1400	Ar	40% CO_2/Ar	671	575	Dey et al. [214]
$Pr_{0.18}Sr_{0.80}Mn_{0.99}O_{2.951}$	TGA	1400	Ar	CO_2/Ar	637.6	255.0	Takalkar et al. [216]
$La_{0.5}Sr_{0.5}MnO_{3-\delta}$	TGA	1400	Ar	50% CO_2/Ar	338.7	684.3	Takalkar et al. [217]

Note: * means that the unit is in mL/g. TGA means thermogravimetric analyzer.

Mulmi et al. [218] used a non-stoichiometric $Ba_2Ca_{0.66}Nb_{1.34-x}Fe_xO_{6-\delta}$perovskite for thermochemical CO generation. An increase of CO generation with Fe content was observed. A perovskite photocatalyst comprising mixed Fe oxides was developed by Zhang et al. [219]. Notably, almost complete CO_2 to CO conversion was reported in the temperature range of 900–980 °C.

A literature summary of various CO_2 conversion perovskite photocatalysts is presented in Table 2. Xu et al. [220] reported the applicability of the $CsPbBr_3$ perovskite quantum dot photocatalyst for solar fuel generation from CO_2. A CO_2 reduction rate of 23.7 μmol/g/h was achieved using this photocatalyst. Moreover, a selectivity of more than 99.3% was discerned. Interestingly, the incorporation of graphene oxide (GO) was beneficial to exceed the electron consumption rate by 25%. Hou et al. [221] also reported analogous observations for $CsPbBr_3$ perovskite quantum dots with a dimension of 3–12 nm. A photocatalyst developed using a mixed halide perovskite, $CsPb(Br_{0.5}/Cl_{0.5})_3$, exhibited high performance in terms of efficiency and CO selectivity [222]. Zhou et al. [223] explored the possibility of the $Cs_2AgBiBr_6$ perovskite for photochemical conversion of CO_2 to solar fuels. For this catalyst, an electron consumption of approximately 105 μmol/g was noted down.

A composite photocatalyst comprising $CsPbBr_3$ perovskite nanocrystals and Pd nanosheets was developed by Xu et al. [224] for CO_2 conversion. With pure $CsPbBr_3$ perovskite nanocrystals, approximately 2.4 times higher electron utilization efficiency was achieved by the incorporation of Pd nanosheets. In another study, Wan et al. [225] developed a $CsPbBr_3$ perovskite quantum dots/UiO-66 (NH_2) nanocomposite photocatalyst exhibiting improved CO_2 reduction activity as well as CO selectivity. Wang et al. [226] prepared a solar-to-CO_2 reduction catalyst by decorating the $PbBiO_2Br$ perovskite with carbonized polymer dots in the presence of a self-sacrificing ionic liquid reaction source. The resultant composite photocatalyst exhibited advantages in CO yield, reliability, and selectivity.

Shan et al. [227] used a boron-doped version of $SrTiO_3$ for photocatalytic conversion of CO_2. It was reported that the photocatalytic activity of boron-doped $SrTiO_3$ enhanced by almost 3-fold by the improvement of charge separation potential. Ag infusion was found beneficial to enhance CO generation of the $H_2SrTa_2O_7$ perovskite photocatalyst, according to the research conducted by Wang et al. [228], owing to reduced reaction overpotential. Accordingly, a CO selectivity of approximately 70% was noted after the infusion of 0.5 wt% Ag. A computational analysis conducted by Hafez et al. [229] supported the suitability of a series of oxynitride perovskites, such as $LaTiO_2N$, TaO_2N with Ba, Sr, or Ca, and NbO_2N with Ba or Sr.

A photocatalyst based on sodium tantalate (V_O-NaTaON) nanocubes exhibiting concurrently enhanced light absorption and charge separation ability was reported by Hou et al. [230]. Consequently, a broad spectrum of photoreduction of CO_2 to fuels was observed for this photocatalyst.

Jang et al. [162] developed a tandem solar cell consisting of the $CH_3NH_3PbI_3$ perovskite and ZnTe photocathode for the selective conversion of CO_2. Notably, a conversion efficiency of more than 0.35% and 0.43% was observed for solar-to-CO and solar-to-fuel conversions, respectively. Wang et al. [231] developed a photocatalyst possessing improved solar-to-fuel conversion performance by graphene oxide decoration of the $CH_3NH_3PbBr_3$ perovskite. As a result, a significant CO yield was obtained on account of enhanced electron extraction and transfer efficiency.

Table 2. Perovskite photocatalysts for CO_2 conversion.

Catalyst	Light Source	Solvent	Products	CO Yield (μmol/g)	CH_4 Yield (μmol/g)	H_2 Yield (μmol/g)	Reference
$CsPbBr_3$ quantum dots (3.05–8.65 nm)	100 W Xe lamp with an AM 1.5 G filter	Ethyl acetate	CO, CH_4, H_2	49.5	22.9	1.07	Xu et al. [220]
$CsPbBr_3$ quantum dots/GO composite	100 W Xe lamp with an AM 1.5 G filter	Ethyl acetate	CO, CH_4, H_2	58.7	29.6	1.58	Xu et al. [220]
$CsPbBr_3$ quantum dots (3–12 nm)	300 W Xe lamp with an AM 1.5 G filter	Ethyl acetate/H_2O	CO, CH_4, H_2	34.1 ± 0.1	12.2 ± 0.1	0.80 ± 0.03	Hou et al. [221]
$CsPb(Br_{0.5}/Cl_{0.5})_3$ nanocrystals	300 W Xe lamp with an AM 1.5 G filter	Ethyl acetate	CO, CH_4	ca. 750	ca. 125	-	Guo et al. [222]
$Cs_2AgBiBr_6$ nanocrystals	100 W Xe lamp with an AM 1.5 G filter	Ethyl acetate	CO, CH_4	14.1	9.6	-	Zhou et al. [223]
$CsPbBr_3$ nanocrystals/Pd nanosheet composite	150 W Xe lamp with with a 420 nm optical filter	H_2O	CO, CH_4, H_2	12.633	3.935	1.167	Xu et al. [224]
$CsPbBr_3$ quantum dots/UiO-66 (NH_2) composite	300 W Xe lamp with a 420 nm UV-cut filter	Ethyl acetate/H_2O	CO, CH_4	98.57	3.08	-	Wan et al. [225]
$PbBiO_2Br$/carbonized polymer dots composite	300 W Xe lamp	H_2O	CO	ca. 48	-	-	Wang et al. [226]
Boron-doped $SrTiO_3$	300 W Xe arc lamp	H_2O	CO, CH_4, O_2	21 *	14 *	-	Shan et al. [227]
Ag-loaded $H_2SrTa_2O_7$	300 W Xe lamp with λ > 200 nm	H_2O	CO, H_2	0.39 *	-	0.25 *	Wang et al. [228]
Sodium tantalate nanocubes	300 W Xe lamp with λ > 400 nm	H_2O	CO, CH_4	75	26	-	Hou et al. [230]
N-doped graphene quantum dots-grafted sodium tantalate nanocubes	300 W Xe lamp with λ > 400 nm	H_2O	CO, CH_4	180	45	-	Hou et al. [230]

Note: * means that the unit is in μmol/h/g.

9. Challenges and Future Directions

Perovskite materials show great promise for CO_2 conversion applications, yet several challenges need to be resolved for large-scale implementation. For example, perovskite cells currently make use of only a small portion of the materials' active sites, thus more efforts on developing large surface area systems using various nanotechnology-based engineering approaches are needed. The design of perovskites providing sustainable performance has also been a challenge. Under thermal stress, in particular, it is imperative for these materials to maintain optimum performance for the desired duration. For instance, solar cells should operate efficiently at temperatures ranging from −40 to +85 °C for long periods of time. On that note, standardized testing protocols for perovskites are necessary. Currently, stability tests may offer valuable clues on the tolerance levels of materials under consideration [148], yet more accurate and reproducible results are required to venture into large-scale production.

New and optimized systems of perovskites with more compositions are also needed to overcome chemical stability and sustained performance issues at high temperatures in CO_2 and H_2O environments. Studies have shown that the ideal perovskite-based solar conversion systems should have fast kinetics, and the "right" thermodynamics to yield in high efficiency during water and CO_2 conversion, while maintaining their mechanical stability. Entropy considerations should be given particular attention, while further comprehension of the tenability degree of perovskites is required using approaches such as computational thermodynamics [154]. The objective is to gain insight about the effects of doping on entropy. Future studies on this matter need to also use approaches such as density functional theory, where the outcome is anticipated to be helpful in the prediction of thermodynamic attributes.

This review also discussed the potential of oxygen carriers in chemical looping, during which a two-step process is carried out, where the selected metal oxides undergo reduction and oxidation; thus, in this case, it is evident that oxides with a high affinity for oxygen are desirable. The objective is to optimize the perovskite materials so that they exhibit stable regeneration capability and achieve sustainable efficiency, while further investigations are required to determine reaction mechanisms and to show mechanical stability for use in industrial chemical looping combustion reactors.

Finally, the use of toxic components in perovskites has been a major concern. Investors require that the issue of material toxicity should be addressed, now that perovskite-based photovoltaic technologies are steadily penetrating various markets. With the growing demand for clean energy, a comprehensive assessment of perovskites is required to determine the most highly performing and least toxic ones. Similarly, the solvents used in the redox reactions should have low toxicity as well. In addition, metals such as silver and gold should be avoided if possible, in order to develop cost-effective systems. Instead, carbon electrodes should be explored as they have proven to be a reliable alternative [232–234].

10. Conclusions

The anthropogenic CO_2 emissions in the atmosphere due to the consumption of fossil fuels has been a critical concern associated with global warming. To this end, the introduction of novel conversion technologies for green production of fuels is expected to suppress the effects of CO_2 accumulation in the atmosphere and simultaneously help meet the globally increasing energy demand. This review presents progress on the use of perovskites for CO_2 conversion and how properties and structural variations can impact the related processes and final products. Current developments reveal promise for these materials, yet also motivate for further studies, particularly with focus on enhancing efficiency, reactivity, selectivity, and stability at high temperatures, reducing cost, increasing throughput, lowering toxicity, reducing energy consumption, establishing reproducibility, and ensuring longer lifetime.

The exploration of CO_2 conversion has led to the discovery or adaptation of useful technologies, such as chemical looping. This process has the potential of producing clean energy through the ability to capture and reduce CO_2; thus, upon large-scale implementation of the technology, economies can have the chance to realize sustainable energy. This realization is heavily based on material development

and nano-engineering with particular efforts dedicated toward optimization of oxygen carriers to significantly enhance efficiency and sustainable performance. The optimization of photovoltaic materials is also underway for application in solar cells, where they catalytically produce photoelectric currents. Yet, the quantity of electricity produced needs to be considerably increased, so that the novel solar cells become competitive and head toward commercialization. To further expand the applicability of perovskite materials for energy and environmental applications, issues such as toxicity need to be addressed as well. Toxicity can be caused inherently by one or more of the components of the perovskite material, such as Pb, as well as the used solvents during operation.

Overall, aside from the challenges experienced in the utilization of perovskites, there are many opportunities to exploit. For instance, the production of hydrogen through water photolysis produces a clean and reliable form of energy, which can be scaled up using photoelectric generators in the solar cells, while the extra heat produced in solar cell operations can be tapped for electricity production. Although R&D continues to discover new applications of perovskites that make these materials more valuable, the biggest challenge is breaking the scalability limitations to fully realize their potential for the production of fuel and valuable chemicals that will significantly contribute toward meeting the future energy, environmental, and sustainability demands.

Funding: This research was funded by the Abu Dhabi National Oil Company R&D division (grant number RDProj.018-GP). The APC was funded by Khalifa University (award RC2-2018-024).

Conflicts of Interest: The authors declare no conflict of interest.

References

1. Li, K.; Peng, B.; Peng, T. Recent advances in heterogeneous photocatalytic CO_2 conversion to solar fuels. *ACS Catal.* **2016**, *6*, 7485–7527. [CrossRef]
2. Zheng, Y.; Zhang, W.; Li, Y.; Chen, J.; Yu, B.; Wang, J.; Zhang, L.; Zhang, J. Energy related CO_2 conversion and utilization: Advanced materials/nanomaterials, reaction mechanisms and technologies. *Nano Energy* **2017**, *40*, 512–539. [CrossRef]
3. Ahmad, W.; Khan, J.; Niu, G.; Tang, J. Inorganic $CsPbI_3$ perovskite-based solar cells: A choice for a tandem device. *Sol. RRL* **2017**, *1*, 1700048. [CrossRef]
4. Andrews, E.M.; Flake, J.; Fang, Y. CO_2 electrocatalytic reduction at gold and copper electrodes: Role of particle size and surface chemistry. *ECS Trans.* **2015**, *66*, 67–70. [CrossRef]
5. Baghel, R.S.; Mantri, V.A.; Reddy, C. A new wave of research interest in marine macroalgae for chemicals and fuels: Challenges and potentials. In *Fuels, Chemicals and Materials from the Oceans and Aquatic Sources*; Kerton, F.M., Yan, N., Eds.; John Wiley & Sons Ltd.: Hoboken, NY, USA, 2017; pp. 43–63.
6. Anastasiou, S.; Bhoria, N.; Pokhrel, J.; Reddy, K.S.K.; Srinivasakannan, C.; Wang, K.; Karanikolos, G.N. Metal-organic framework/graphene oxide composite fillers in mixed-matrix membranes for CO_2 separation. *Mater. Chem. Phys.* **2018**, *212*, 513–522. [CrossRef]
7. Pokhrel, J.; Bhoria, N.; Anastasiou, S.; Tsoufis, T.; Gournis, D.; Romanos, G.; Karanikolos, G.N. CO_2 adsorption behavior of amine-functionalized ZIF-8, graphene oxide, and ZIF-8/graphene oxide composites under dry and wet conditions. *Microporous Mesoporous Mater.* **2018**, *267*, 53–67. [CrossRef]
8. Varghese, A.; Mittal, V. Performance of various adsorbents towards diverse gases: A comparative study. In *Functional Nanomaterials and Nanotechnologies: Applications for Energy & Environment*; Central West Publishing: Orange, NSW, Australia, 2018; pp. 305–404.
9. Behar, O. Solar thermal power plants—A review of configurations and performance comparison. *Renew. Sustain. Energy Rev.* **2018**, *92*, 608–627. [CrossRef]
10. Bhati, M.; Rai, R. Commercialization of large-scale perovskite solar energy technology and scaling-up issues. In *Perovskite Photovoltaics*; Elsevier: Amsterdam, The Netherlands, 2018; pp. 387–445.
11. Bijarniya, J.P.; Sudhakar, K.; Baredar, P. Concentrated solar power technology in India: A review. *Renew. Sustain. Energy Rev.* **2016**, *63*, 593–603. [CrossRef]
12. Bisquert, J.; Garcia-Belmonte, G.; Guerrero, A. Impedance characteristics of hybrid organometal halide perovskite solar cells. In *Organic-Inorganic Halide Perovskite Photovoltaics: From Fundamentals to Device Architectures*; Springer: Cham, Switzerland, 2016; pp. 163–199.

13. Brendelberger, S.; Sattler, C. Concept analysis of an indirect particle-based redox process for solar-driven H_2O/CO_2 splitting. *Sol. Energy* **2015**, *113*, 158–170. [CrossRef]
14. Calió, L.; Kazim, S.; Grätzel, M.; Ahmad, S. Hole-transport materials for perovskite solar cells. *Angew. Chem. Int. Ed.* **2016**, *55*, 14522–14545. [CrossRef]
15. Chatzichristodoulou, C.; Chen, M.; Hendriksen, P.V.; Jacobsen, T.; Mogensen, M.B. Understanding degradation of solid oxide electrolysis cells through modeling of electrochemical potential profiles. *Electrochimica Acta* **2016**, *189*, 265–282. [CrossRef]
16. Chen, H.; Yang, S. Carbon-based perovskite solar cells without hole transport materials: The front runner to the market? *Adv. Mater.* **2017**, *29*, 1603994. [CrossRef]
17. Chen, P.; Bai, Y.; Lyu, M.; Yun, J.H.; Hao, M.; Wang, L. Progress and perspective in low-dimensional metal halide perovskites for optoelectronic applications. *Sol. RRL* **2018**, *2*, 1700186. [CrossRef]
18. Chen, S.; Pan, B.; Zeng, L.; Luo, S.; Wang, X.; Su, W. $La_2Sn_2O_7$ enhanced photocatalytic CO_2 reduction with H_2O by deposition of Au co-catalyst. *RSC Adv.* **2017**, *7*, 14186–14191. [CrossRef]
19. Ezbiri, M.; Takacs, M.; Stolz, B.; Lungthok, J.; Steinfeld, A.; Michalsky, R. Design principles of perovskites for solar-driven thermochemical splitting of CO_2. *J. Mater. Chem. A* **2017**, *5*, 15105–15115. [CrossRef]
20. Zhao, Y.; Waterhouse, G.I.; Chen, G.; Xiong, X.; Wu, L.-Z.; Tung, C.-H.; Zhang, T. Two-dimensional-related catalytic materials for solar-driven conversion of CO_x into valuable chemical feedstocks. *Chem. Soc. Rev.* **2019**, *48*, 1972–2010. [CrossRef]
21. Salhi, B.; Wudil, Y.; Hossain, M.; Al-Ahmed, A.; Al-Sulaiman, F. Review of recent developments and persistent challenges in stability of perovskite solar cells. *Renew. Sustain. Energy Rev.* **2018**, *90*, 210–222. [CrossRef]
22. Wang, J.; Di Giacomo, F.; Brüls, J.; Gorter, H.; Katsouras, I.; Groen, P.; Janssen, R.A.; Andriessen, R.; Galagan, Y. Highly efficient perovskite solar cells using non-toxic industry compatible solvent system. *Sol. RRL* **2017**, *1*, 1700091. [CrossRef]
23. Shi, R.; Waterhouse, G.I.; Zhang, T. Recent progress in photocatalytic CO_2 reduction over perovskite oxides. *Sol. RRL* **2017**, *1*, 1700126. [CrossRef]
24. Wang, Y.; Lv, Z.; Zhou, L.; Chen, X.; Chen, J.; Zhou, Y.; Roy, V.; Han, S.-T. Emerging perovskite materials for high density data storage and artificial synapses. *J. Mater. Chem. C* **2018**, *6*, 1600–1617. [CrossRef]
25. Tu, W.; Zhou, Y.; Zou, Z. Photocatalytic conversion of CO_2 into renewable hydrocarbon fuels: State-of-the-art accomplishment, challenges, and prospects. *Adv. Mater.* **2014**, *26*, 4607–4626. [CrossRef] [PubMed]
26. Kubicek, M.; Bork, A.H.; Rupp, J.L. Perovskite oxides—A review on a versatile material class for solar-to-fuel conversion processes. *J. Mater. Chem. A* **2017**, *5*, 11983–12000. [CrossRef]
27. Risch, M. Perovskite electrocatalysts for the oxygen reduction reaction in alkaline media. *Catalysts* **2017**, *7*, 154. [CrossRef]
28. Yun, S.; Qin, Y.; Uhl, A.R.; Vlachopoulos, N.; Yin, M.; Li, D.; Han, X.; Hagfeldt, A. New-generation integrated devices based on dye-sensitized and perovskite solar cells. *Energy Environ. Sci.* **2018**, *11*, 476–526. [CrossRef]
29. Zheng, Y.; Wang, J.; Yu, B.; Zhang, W.; Chen, J.; Qiao, J.; Zhang, J. A review of high temperature co-electrolysis of H_2O and CO_2 to produce sustainable fuels using solid oxide electrolysis cells (SOECs): Advanced materials and technology. *Chem. Soc. Rev.* **2017**, *46*, 1427–1463. [CrossRef]
30. Yang, M.-Q.; Xu, Y.-J. Photocatalytic conversion of CO_2 over graphene-based composites: Current status and future perspective. *Nanoscale Horiz.* **2016**, *1*, 185–200. [CrossRef]
31. Sahara, G.; Kumagai, H.; Maeda, K.; Kaeffer, N.; Artero, V.; Higashi, M.; Abe, R.; Ishitani, O. Photoelectrochemical reduction of CO_2 coupled to water oxidation using a photocathode with a Ru(II)–Re(I) complex photocatalyst and a CoO_x/TaON Photoanode. *J. Am. Chem. Soc.* **2016**, *138*, 14152–14158. [CrossRef]
32. Costentin, C.; Robert, M.; Savéant, J.-M. Catalysis of the electrochemical reduction of carbon dioxide. *Chem. Soc. Rev.* **2013**, *42*, 2423–2436. [CrossRef]
33. Ganesh, I. Electrochemical conversion of carbon dioxide into renewable fuel chemicals—The role of nanomaterials and the commercialization. *Renew. Sustain. Energy Rev.* **2016**, *59*, 1269–1297. [CrossRef]
34. Atsonios, K.; Panopoulos, K.D.; Kakaras, E. Thermocatalytic CO_2 hydrogenation for methanol and ethanol production: Process improvements. *Int. J. Hydrogen Energy* **2016**, *41*, 792–806. [CrossRef]
35. Smestad, G.P.; Steinfeld, A. photochemical and thermochemical production of solar fuels from H_2O and CO_2 using metal oxide catalysts. *Ind. Eng. Chem. Res.* **2012**, *51*, 11828–11840. [CrossRef]
36. Wei-Guang, D.E.; Chao-Yu, C.P. *Perovskite Solar Cells: Principle, Materials and Devices*; World Scientific: Singapore, 2017; Volume 1.

37. Dolganov, A.; Tanaseichuk, B.; Ivantsova, P.; Tsebulaeva, Y.; Kostrukov, S.; Moiseeva, D.; Shmelkova, N.; Yurova, V.; Balakireva, O.; Trushkova, N. Metal-free electrocatalyst for hydrogen production from water. *Int. J. Electrochem. Sci.* **2016**, *11*, 9559–9565. [CrossRef]
38. Kanhere, P.; Chen, Z. A review on visible light active perovskite-based photocatalysts. *Molecules* **2014**, *19*, 19995–20022. [CrossRef] [PubMed]
39. Wang, W.; Tadé, M.O.; Shao, Z. Research progress of perovskite materials in photocatalysis-and photovoltaics-related energy conversion and environmental treatment. *Chem. Soc. Rev.* **2015**, *44*, 5371–5408. [CrossRef]
40. Wang, M.; Zheng, D.; Ye, M.; Zhang, C.; Xu, B.; Lin, C.; Sun, L.; Lin, Z. One-dimensional densely aligned perovskite-decorated semiconductor heterojunctions with enhanced photocatalytic activity. *Small* **2015**, *11*, 1436–1442. [CrossRef] [PubMed]
41. Qu, Y.; Zhou, W.; Ren, Z.; Du, S.; Meng, X.; Tian, G.; Pan, K.; Wang, G.; Fu, H. Facile preparation of porous $NiTiO_3$ nanorods with enhanced visible-light-driven photocatalytic performance. *J. Mater. Chem.* **2012**, *22*, 16471–16476. [CrossRef]
42. Döscher, H.; Geisz, J.; Deutsch, T.; Turner, J. Sunlight absorption in water–efficiency and design implications for photoelectrochemical devices. *Energy Environ. Sci.* **2014**, *7*, 2951–2956. [CrossRef]
43. Fan, R.; Zhou, N.; Zhang, L.; Yang, R.; Meng, Y.; Li, L.; Guo, T.; Chen, Y.; Xu, Z.; Zheng, G. Toward full solution processed perovskite/Si monolithic tandem solar device with PCE exceeding 20%. *Sol. RRL* **2017**, *1*, 1700149. [CrossRef]
44. Zhang, M.; Lyu, M.; Chen, P.; Hao, M.; Yun, J.H.; Wang, L. Recent advances in low-toxic lead-free metal halide perovskite materials for solar cell application. *Asia-Pac. J. Chem. Eng.* **2016**, *11*, 392–398. [CrossRef]
45. Zhang, Z.; Qin, J.; Shi, W.; Liu, Y.; Zhang, Y.; Liu, Y.; Gao, H.; Mao, Y. Enhanced power conversion efficiency of perovskite solar cells with an up-conversion material of Er^{3+}-Yb^{3+}-Li^{+} tri-doped TiO_2. *Nanoscale Res. Lett.* **2018**, *13*, 147. [CrossRef]
46. Maiti, D.; Hare, B.J.; Daza, Y.A.; Ramos, A.E.; Kuhn, J.N.; Bhethanabotla, V.R. Earth abundant perovskite oxides for low temperature CO_2 conversion. *Energy Environ. Sci.* **2018**, *11*, 648–659. [CrossRef]
47. Ibn-Mohammed, T.; Koh, S.; Reaney, I.; Acquaye, A.; Schileo, G.; Mustapha, K.; Greenough, R. Perovskite solar cells: An integrated hybrid lifecycle assessment and review in comparison with other photovoltaic technologies. *Renew. Sustain. Energy Rev.* **2017**, *80*, 1321–1344. [CrossRef]
48. Zhu, L.; Lu, Y. Reactivity and efficiency of ceria-based oxides for solar CO_2 splitting via isothermal and near-isothermal cycles. *Energy Fuels* **2017**, *32*, 736–746. [CrossRef]
49. Guo, Z.; Gao, L.; Zhang, C.; Xu, Z.; Ma, T. Low-temperature processed non-TiO_2 electron selective layers for perovskite solar cells. *J. Mater. Chem. A* **2018**, *6*, 4572–4589. [CrossRef]
50. Gupta, K.; Bersani, M.; Darr, J.A. Highly efficient electro-reduction of CO_2 to formic acid by nano-copper. *J. Mater. Chem. A* **2016**, *4*, 13786–13794. [CrossRef]
51. Hathaway, B.J.; Bala Chandran, R.; Gladen, A.C.; Chase, T.R.; Davidson, J.H. Demonstration of a solar reactor for carbon dioxide splitting via the isothermal ceria redox cycle and practical implications. *Energy Fuels* **2016**, *30*, 6654–6661. [CrossRef]
52. He, J.; Bi, E.; Tang, W.; Wang, Y.; Zhou, Z.; Yang, X.; Chen, H.; Han, L. Ligand-free, highly dispersed NiO_x nanocrystal for efficient, stable, low-temperature processable perovskite solar cells. *Sol. RRL* **2018**, *2*, 1800004. [CrossRef]
53. Hori, Y. CO_2 Reduction using electrochemical approach. In *Solar to Chemical Energy Conversion: Theory and Application*; Springer: Cham, Switzerland, 2016; pp. 191–211.
54. Hossain, M.I.; Qarony, W.; Jovanov, V.; Tsang, Y.H.; Knipp, D. Nanophotonic design of perovskite/silicon tandem solar cells. *J. Mater. Chem. A* **2018**, *6*, 3625–3633. [CrossRef]
55. Huang, C.; Li, Z.; Zou, Z. A perspective on perovskite oxide semiconductor catalysts for gas phase photoreduction of carbon dioxide. *MRS Commun.* **2016**, *6*, 216–225. [CrossRef]
56. Hu, J.; Cheng, Q.; Fan, R.; Zhou, H. Recent development of organic–inorganic perovskite-based tandem solar cells. *Sol. RRL* **2017**, *1*, 1700045. [CrossRef]
57. Di Giacomo, F.; Galagan, Y.; Shanmugam, S.; Gorter, H.; van den Bruele, F.; Kirchner, G.; de Vries, I.; Fledderus, H.; Lifka, H.; Veenstra, S. Up-scaling perovskite solar cell manufacturing from sheet-to-sheet to roll-to-roll: Challenges and solutions. In Proceedings of the Organic, Hybrid, and Perovskite Photovoltaics XVIII, San Diego, CA, USA, 6–10 August 2017.

58. Dias, P.; Mendes, A. Hydrogen production from photoelectrochemical water splitting. In *Fuel Cells and Hydrogen Production: A Volume in the Encyclopedia of Sustainability Science and Technology*, 2nd ed.; Lipman, T.E., Weber, A., Eds.; Springer-Verlag: New York, NY, USA, 2019; pp. 1003–1053.
59. Williams, S.T.; Chueh, C.C.; Jen, A.K.Y. Navigating organo-lead halide perovskite phase space via nucleation kinetics toward a deeper understanding of perovskite phase transformations and structure–property relationships. *Small* **2015**, *11*, 3088–3096. [CrossRef] [PubMed]
60. Zhu, X.; Liu, Z.; Ming, N. Perovskite oxide nanotubes: Synthesis, structural characterization, properties and applications. *J. Mater. Chem.* **2010**, *20*, 4015–4030. [CrossRef]
61. Choi, J.J.; Yang, X.; Norman, Z.M.; Billinge, S.J.; Owen, J.S. Structure of methylammonium lead iodide within mesoporous titanium dioxide: Active material in high-performance perovskite solar cells. *Nano Lett.* **2013**, *14*, 127–133. [CrossRef] [PubMed]
62. Colonna, S.; De Rossi, S.; Faticanti, M.; Pettiti, I.; Porta, P. Zirconia supported La, Co oxides and $LaCoO_3$ perovskite: Structural characterization and catalytic CO oxidation. *J. Mol. Catal. A Chem.* **2002**, *180*, 161–168. [CrossRef]
63. Crumlin, E.J.; Mutoro, E.; Liu, Z.; Grass, M.E.; Biegalski, M.D.; Lee, Y.-L.; Morgan, D.; Christen, H.M.; Bluhm, H.; Shao-Horn, Y. Surface strontium enrichment on highly active perovskites for oxygen electrocatalysis in solid oxide fuel cells. *Energy Environ. Sci.* **2012**, *5*, 6081–6088. [CrossRef]
64. Keav, S.; Matam, S.; Ferri, D.; Weidenkaff, A. Structured perovskite-based catalysts and their application as three-way catalytic converters—A review. *Catalysts* **2014**, *4*, 226–255. [CrossRef]
65. Avila, P.; Montes, M.; Miró, E.E. Monolithic reactors for environmental applications: A review on preparation technologies. *Chem. Eng. J.* **2005**, *109*, 11–36. [CrossRef]
66. Tanaka, H.; Taniguchi, M.; Uenishi, M.; Kajita, N.; Tan, I.; Nishihata, Y.; Mizuki, J.I.; Narita, K.; Kimura, M.; Kaneko, K. Self-regenerating Rh-and Pt-based perovskite catalysts for automotive-emissions control. *Angew. Chem. Int. Ed.* **2006**, *45*, 5998–6002. [CrossRef]
67. Abdelhady, A.L.; Saidaminov, M.I.; Murali, B.; Adinolfi, V.; Voznyy, O.; Katsiev, K.; Alarousu, E.; Comin, R.; Dursun, I.; Sinatra, L. Heterovalent dopant incorporation for bandgap and type engineering of perovskite crystals. *J. Phys. Chem. Lett.* **2016**, *7*, 295–301. [CrossRef]
68. Kueh, B.; Kapsi, M.; Veziri, C.M.; Athanasekou, C.; Pilatos, G.; Reddy, K.S.K.; Raj, A.; Karanikolos, G.N. Asphaltene-derived activated carbon and carbon nanotube membranes for CO_2 separation. *Energy Fuels* **2018**, *32*, 11718–11730. [CrossRef]
69. Kontos, A.G.; Likodimos, V.; Veziri, C.M.; Kouvelos, E.; Moustakas, N.; Karanikolos, G.N.; Romanos, G.E.; Falaras, P. CO_2 captured in zeolitic imidazolate frameworks: Raman spectroscopic analysis of uptake and host–guest interactions. *ChemSusChem* **2014**, *7*, 1696–1702. [CrossRef] [PubMed]
70. Stoeger, J.A.; Palomino, M.; Agrawal, K.V.; Zhang, X.; Karanikolos, G.N.; Valencia, S.; Corma, A.; Tsapatsis, M. Oriented CoSAPO-5 membranes by microwave-enhanced growth on TiO_2-coated porous alumina. *Angew. Chem. Int. Ed.* **2012**, *51*, 2470–2473. [CrossRef] [PubMed]
71. Langørgen, Ø.; Saanum, I.; Haugen, N.E.L. Chemical looping combustion of methane using a copper-based oxygen carrier in a 150 kW reactor system. *Energy Procedia* **2017**, *114*, 352–360. [CrossRef]
72. Nadarajah, A. *Fabrication and Processing of Next-Generation Oxygen Carrier Materials for Chemical Looping Combustion*; Technical Report No. DE-FE0008774; University of Toledo: Toledo, OH, USA, 2017.
73. Pishahang, M.; Larring, Y.; Sunding, M.; Jacobs, M.; Snijkers, F. Performance of perovskite-type oxides as oxygen-carrier materials for chemical looping combustion in the presence of H_2S. *Energy Technol.* **2016**, *4*, 1305–1316. [CrossRef]
74. Figueroa, J.D.; Fout, T.; Plasynski, S.; McIlvried, H.; Srivastava, R.D. Advances in CO_2 capture technology—The US Department of Energy's Carbon Sequestration Program. *Int. J. Greenh. Gas Control* **2008**, *2*, 9–20. [CrossRef]
75. Goel, M. CO_2 Capture and utilization for the energy industry: Outlook for capability development to address climate change in India. In *Carbon Utilization—Applications for the Energy Industry*; Springer: Singapore, 2017; pp. 3–33.
76. Yeh, S.; Rubin, E.S. A review of uncertainties in technology experience curves. *Energy Econ.* **2012**, *34*, 762–771. [CrossRef]
77. Fan, L.-S.; Zeng, L.; Wang, W.; Luo, S. Chemical looping processes for CO_2 capture and carbonaceous fuel conversion—Prospect and opportunity. *Energy Environ. Sci.* **2012**, *5*, 7254–7280. [CrossRef]

78. Han, L.; Lin, M.; Haussener, S. Reliable performance characterization of mediated photocatalytic water-splitting half reactions. *ChemSusChem* **2017**, *10*, 2158–2166. [CrossRef]
79. Hu, J.; Galvita, V.; Poelman, H.; Marin, G. Advanced chemical looping materials for CO_2 utilization: A review. *Materials* **2018**, *11*, 1187. [CrossRef]
80. Fan, L.S.; Zeng, L.; Luo, S. Chemical-looping technology platform. *AIChE J.* **2015**, *61*, 2–22. [CrossRef]
81. Bhavsar, S.; Veser, G.T. Reducible supports for Ni-based oxygen carriers in chemical looping combustion. *Energy Fuels* **2013**, *27*, 2073–2084. [CrossRef]
82. Liu, G.; He, D.; Yao, R.; Zhao, Y.; Li, J. Amorphous NiFeB nanoparticles realizing highly active and stable oxygen evolving reaction for water splitting. *Nano Res.* **2018**, *11*, 1664–1675. [CrossRef]
83. Jamesh, M.I. Recent progress on earth abundant hydrogen evolution reaction and oxygen evolution reaction bifunctional electrocatalyst for overall water splitting in alkaline media. *J. Power Sources* **2016**, *333*, 213–236. [CrossRef]
84. Serrano, A.; García-Labiano, F.; de Diego, L.; Gayán, P.; Abad, A.; Adánez, J. Chemical Looping Combustion of liquid fossil fuels in a 1 kWth unit using a Fe-based oxygen carrier. *Fuel Process. Technol.* **2017**, *160*, 47–54. [CrossRef]
85. Thursfield, A.; Murugan, A.; Franca, R.; Metcalfe, I.S. Chemical looping and oxygen permeable ceramic membranes for hydrogen production—A review. *Energy Environ. Sci.* **2012**, *5*, 7421–7459. [CrossRef]
86. Kwak, B.S.; Park, N.-K.; Ryu, S.O.; Baek, J.-I.; Ryu, H.-J.; Kang, M. Improved reversible redox cycles on MTiOx (M = Fe, Co, Ni, and Cu) particles afforded by rapid and stable oxygen carrier capacity for use in chemical looping combustion of methane. *Chem. Eng. J.* **2017**, *309*, 617–627. [CrossRef]
87. Ito, S. Inorganic hole-transporting materials for perovskite solar cell. In *Organic-Inorganic Halide Perovskite Photovoltaics*; Park, N.-G., Grätzel, M., Miyasaka, T., Eds.; Springer: Cham, Switzerland, 2016; pp. 343–366.
88. Gayán, P.; Luis, F.; García-Labiano, F.; Adánez, J.; Abad, A.; Dueso, C. Effect of support on reactivity and selectivity of Ni-based oxygen carriers for chemical-looping combustion. *Fuel* **2008**, *87*, 2641–2650. [CrossRef]
89. Dueso, C.; Ortiz, M.; Abad, A.; García-Labiano, F.; Luis, F.; Gayán, P.; Adánez, J. Reduction and oxidation kinetics of nickel-based oxygen-carriers for chemical-looping combustion and chemical-looping reforming. *Chem. Eng. J.* **2012**, *188*, 142–154. [CrossRef]
90. Rydén, M.; Lyngfelt, A.; Mattisson, T. Chemical-looping combustion and chemical-looping reforming in a circulating fluidized-bed reactor using Ni-based oxygen carriers. *Energy Fuels* **2008**, *22*, 2585–2597. [CrossRef]
91. Luis, F.; Ortiz, M.; Adánez, J.; García-Labiano, F.; Abad, A.; Gayán, P. Synthesis gas generation by chemical-looping reforming in a batch fluidized bed reactor using Ni-based oxygen carriers. *Chem. Eng. J.* **2008**, *144*, 289–298.
92. Ipsakis, D.; Heracleous, E.; Silvester, L.; Bukur, D.; Lemonidou, A. Kinetic modeling of NiO-based oxygen carriers for the sorption enhanced chemical looping steam CH_4 reforming. *Mater. Today Proc.* **2018**, *5*, 27353–27361. [CrossRef]
93. Tijani, M.M.A.A. Study of the Methane Chemical Looping Combustion Process Using Supported Metal Carriers for Carbon Capture. Ph.D. Thesis, University of Calgary, Calgary, AB, Canada, November 2018.
94. Park, J.H.; Hwang, R.H.; ur Rasheed, H.; Baek, J.I.; Ryu, H.J.; Yi, K.B. Kinetics of the reduction and oxidation of Mg added NiO/Al_2O_3 for chemical looping combustion. *Chem. Eng. Res. Des.* **2019**, *141*, 481–491. [CrossRef]
95. Choudhary, V.; Uphade, B.; Mamman, A. Oxidative conversion of methane to syngas over nickel supported on commercial low surface area porous catalyst carriers precoated with alkaline and rare earth oxides. *J. Catal.* **1997**, *172*, 281–293. [CrossRef]
96. Wang, S.; Lu, G. A comprehensive study on carbon dioxide reforming of methane over Ni/γ-Al_2O_3 catalysts. *Ind. Eng. Chem. Res.* **1999**, *38*, 2615–2625. [CrossRef]
97. Chen, S.; Lior, N.; Xiang, W. Coal gasification integration with solid oxide fuel cell and chemical looping combustion for high-efficiency power generation with inherent CO_2 capture. *Appl. Energy* **2015**, *146*, 298–312. [CrossRef]
98. Gayán, P.; Dueso, C.; Abad, A.; Adanez, J.; Luis, F.; García-Labiano, F. NiO/Al_2O_3 oxygen carriers for chemical-looping combustion prepared by impregnation and deposition–precipitation methods. *Fuel* **2009**, *88*, 1016–1023. [CrossRef]
99. Sedor, K.E.; Hossain, M.M.; de Lasa, H.I. Reactivity and stability of Ni/Al_2O_3 oxygen carrier for chemical-looping combustion (CLC). *Chem. Eng. Sci.* **2008**, *63*, 2994–3007. [CrossRef]

100. Yu, L.; Song, M.; Williams, P.T.; Wei, Y. Alumina-supported spinel Ni Al_2O_4 as a catalyst for reforming pyrolysis gas. *Ind. Eng. Chem. Res.* **2019**, *58*, 11770–11778. [CrossRef]
101. Beierlein, D.; Häussermann, D.; Pfeifer, M.; Schwarz, T.; Stöwe, K.; Traa, Y.; Klemm, E. Is the CO_2 methanation on highly loaded Ni-Al_2O_3 catalysts really structure-sensitive? *Appl. Catal. B Environ.* **2019**, *247*, 200–219. [CrossRef]
102. Baek, J.-I.; Kim, U.; Jo, H.; Eom, T.H.; Lee, J.B.; Ryu, H.-J. Effect of Mg–Al layered double hydroxide use on the performance of a spray-dried NiO oxygen carrier. *J. Chem. Eng. Jpn.* **2018**, *51*, 596–604. [CrossRef]
103. Adánez, J.; García-Labiano, F.; Abad, A.; de Diego, L.; Gayán, P.; Dueso, C. NiO-based oxygen carriers impregnated on Al_2O_3-based materials for chemical-looping combustion. In *Carbon Dioxide Capture for Storage in Deep Geological Formations—Results from the CO_2 Capture Project*; Eide, L.I., Ed.; CPL Press: Newbury, UK, 2009; Volume 3, pp. 85–94.
104. Shervedani, R.K.; Torabi, M.; Yaghoobi, F. Binder-free prickly nickel nanostructured/reduced graphene oxide composite: A highly efficient electrocatalyst for hydrogen evolution reaction in alkaline solutions. *Electrochim. Acta* **2017**, *244*, 230–238. [CrossRef]
105. Roux, S.; Bensakhria, A.; Antonini, G. Study and improvement of the regeneration of metallic oxides used as oxygen carriers for a new combustion process. *Int. J. Chem. React. Eng.* **2006**, *4*, 1542–6580. [CrossRef]
106. Wei, Y. Syngas generation from methane using a chemical-looping concept: A review of oxygen carriers. *J. Chem.* **2013**, *2013*, 294817.
107. Ahmed, W.; Awadallah, A.E.; Aboul-Enein, A.A. Ni/CeO_2–Al_2O_3 catalysts for methane thermo-catalytic decomposition to CO_x-free H_2 production. *Int. J. Hydrogen Energy* **2016**, *41*, 18484–18493. [CrossRef]
108. Yonggang, W.; Hua, W.; Kongzhai, L.; Xing, Z.; Yunpeng, D. Preparation and characterization of Ce_{1-x} Ni_xO_2 as oxygen carrier for selective oxidation methane to syngas in absence of gaseous oxygen. *J. Rare Earths* **2010**, *28*, 357–361.
109. Du, X.; Zhang, D.; Shi, L.; Gao, R.; Zhang, J. Morphology dependence of catalytic properties of Ni/CeO_2 nanostructures for carbon dioxide reforming of methane. *J. Phys. Chem. C* **2012**, *116*, 10009–10016. [CrossRef]
110. Hossain, M.M. Solid-state kinetics of reduction of NiO/Ce–γAl_2O_3 oxygen carriers for chemical-looping combustion. *Arab. J. Sci. Eng.* **2018**, *43*, 2281–2290. [CrossRef]
111. Zhao, X.; Ngo, H.T.; Walker, D.M.; Weber, D.; Maiti, D.; Cimenler, U.; Petrov, A.D.; Joseph, B.; Kuhn, J.N. Tri-reforming of surrogate biogas over Ni/Mg/ceria–zirconia/alumina pellet catalysts. *Chem. Eng. Commun.* **2018**, *205*, 1129–1142. [CrossRef]
112. Abad, A.; Mattisson, T.; Lyngfelt, A.; Johansson, M. The use of iron oxide as oxygen carrier in a chemical-looping reactor. *Fuel* **2007**, *86*, 1021–1035. [CrossRef]
113. Ma, S.; Chen, S.; Soomro, A.; Xiang, W. Effects of supports on hydrogen production and carbon deposition of Fe-based oxygen carriers in chemical looping hydrogen generation. *Int. J. Hydrogen Energy* **2017**, *42*, 11006–11016. [CrossRef]
114. Bhui, B.; Vairakannu, P. Experimental and kinetic studies on in-situ CO_2 gasification based chemical looping combustion of low ash coal using Fe_2O_3 as the oxygen carrier. *J. CO_2 Util.* **2019**, *29*, 103–116. [CrossRef]
115. Hu, S.; Chen, Q.; Xiang, J.; Su, S.; Sun, L.; Wang, Y.; Xu, B.; Chi, H. Modification of iron oxide to promote reaction property for chemical looping combustion with CO. *Combust. Sci. Technol.* **2016**, *188*, 1319–1330. [CrossRef]
116. De Diego, L.F.; Serrano, A.; García-Labiano, F.; García-Díez, E.; Abad, A.; Gayán, P.; Adánez, J. Bioethanol combustion with CO_2 capture in a 1 kWth Chemical Looping Combustion prototype: Suitability of the oxygen carrier. *Chem. Eng. J.* **2016**, *283*, 1405–1413. [CrossRef]
117. Karimi, E.; Forutan, H.; Saidi, M.; Rahimpour, M.; Shariati, A. Experimental study of chemical-looping reforming in a fixed-bed reactor: Performance investigation of different oxygen carriers on Al_2O_3 and TiO_2 support. *Energy Fuels* **2014**, *28*, 2811–2820. [CrossRef]
118. Hafizi, A.; Rahimpour, M.; Hassanajili, S. Calcium promoted Fe/Al_2O_3 oxygen carrier for hydrogen production via cyclic chemical looping steam methane reforming process. *Int. J. Hydrogen Energy* **2015**, *40*, 16159–16168. [CrossRef]
119. Siriwardane, R.; Tian, H.; Miller, D.; Richards, G. Fluidized bed testing of commercially prepared MgO-promoted hematite and CuO–Fe_2O_3 mixed metal oxide oxygen carriers for methane and coal chemical looping combustion. *Appl. Energy* **2015**, *157*, 348–357. [CrossRef]

120. Hafizi, A.; Rahimpour, M.; Hassanajili, S. High purity hydrogen production via sorption enhanced chemical looping reforming: Application of $22Fe_2O_3/MgAl_2O_4$ and $22Fe_2O_3/Al_2O_3$ as oxygen carriers and cerium promoted CaO as CO_2 sorbent. *Appl. Energy* **2016**, *169*, 629–641. [CrossRef]
121. Liu, Y.-C.; Ku, Y.; Tseng, Y.-H.; Lee, H.-Y.; Kuo, Y.-L. Fabrication of Fe_2O_3/TiO_2 oxygen carriers for chemical looping combustion and hydrogen generation. *Aerosol Air Qual. Res* **2016**, *16*, 2023–2032. [CrossRef]
122. Tang, M.; Liu, K.; Roddick, D.M.; Fan, M. Enhanced lattice oxygen reactivity over Fe_2O_3/Al_2O_3 redox catalyst for chemical-looping dry (CO_2) reforming of CH_4: Synergistic La-Ce effect. *J. Catal.* **2018**, *368*, 38–52. [CrossRef]
123. Hu, J.; Galvita, V.V.; Poelman, H.; Detavernier, C.; Marin, G.B. A core-shell structured $Fe_2O_3/ZrO_2@ZrO_2$ nanomaterial with enhanced redox activity and stability for CO_2 conversion. *J. CO_2 Util.* **2017**, *17*, 20–31. [CrossRef]
124. Pérez-Vega, R.; Abad, A.; Gayán, P.; de Diego, L.; García-Labiano, F.; Adánez, J. Development of $(Mn_{0.77}Fe_{0.23})_2O_3$ particles as an oxygen carrier for coal combustion with CO_2 capture via in-situ gasification chemical looping combustion (*i*G-CLC) aided by oxygen uncoupling (CLOU). *Fuel Process. Technol.* **2017**, *164*, 69–79.
125. Pérez-Vega, R.; Abad, A.; Izquierdo, M.; Gayán, P.; de Diego, L.; Adánez, J. Evaluation of Mn-Fe mixed oxide doped with TiO_2 for the combustion with CO_2 capture by Chemical Looping assisted by Oxygen Uncoupling. *Appl. Energy* **2019**, *237*, 822–835. [CrossRef]
126. Lee, Y.Y.; Jung, H.S.; Kang, Y.T. A review: Effect of nanostructures on photocatalytic CO_2 conversion over metal oxides and compound semiconductors. *J. CO_2 Util.* **2017**, *20*, 163–177. [CrossRef]
127. Liu, F.; Chen, L.; Neathery, J.K.; Saito, K.; Liu, K. Cerium oxide promoted iron-based oxygen carrier for chemical looping combustion. *Ind. Eng. Chem. Res.* **2014**, *53*, 16341–16348. [CrossRef]
128. Kang, D.; Lee, M.; Lim, H.S.; Lee, J.W. Chemical looping partial oxidation of methane with CO_2 utilization on the ceria-enhanced mesoporous Fe_2O_3 oxygen carrier. *Fuel* **2018**, *215*, 787–798. [CrossRef]
129. Hafizi, A.; Jafari, M.; Rahimpour, M.; Hassanajili, S. Experimental investigation of sorption enhanced chemical looping reforming for high purity hydrogen production using CeO_2–CaO CO_2 sorbent and 15Fe–5Ca/Al_2O_3 oxygen carrier. *J. Taiwan Inst. Chem. Eng.* **2016**, *65*, 185–196. [CrossRef]
130. Kuo, Y.-L.; Huang, W.-C.; Hsu, W.-M.; Tseng, Y.-H.; Ku, Y. Use of spinel nickel aluminium ferrite as self-supported oxygen carrier for chemical looping hydrogen generation process. *Aerosol Air Qual. Res.* **2015**, *15*, 2700–2708. [CrossRef]
131. Zaabout, A.; Dahl, P.I.; Ugwu, A.; Tolchard, J.R.; Cloete, S.; Amini, S. Gas Switching Reforming (GSR) for syngas production with integrated CO_2 capture using iron-based oxygen carriers. *Int. J. Greenh. Gas Control* **2019**, *81*, 170–180. [CrossRef]
132. Hu, J.; Buelens, L.; Theofanidis, S.-A.; Galvita, V.V.; Poelman, H.; Marin, G.B. CO_2 conversion to CO by auto-thermal catalyst-assisted chemical looping. *J. CO_2 Util.* **2016**, *16*, 8–16. [CrossRef]
133. Huang, X.; Wang, X.; Fan, M.; Wang, Y.; Adidharma, H.; Gasem, K.A.; Radosz, M. A cost-effective approach to reducing carbon deposition and resulting deactivation of oxygen carriers for improvement of energy efficiency and CO_2 capture during methane chemical-looping combustion. *Appl. Energy* **2017**, *193*, 381–392. [CrossRef]
134. Pérez-Vega, R.; Adánez-Rubio, I.; Gayán, P.; Izquierdo, M.T.; Abad, A.; García-Labiano, F.; Luis, F.; Adánez, J. Sulphur, nitrogen and mercury emissions from coal combustion with CO_2 capture in chemical looping with oxygen uncoupling (CLOU). *Int. J. Greenh. Gas Control* **2016**, *46*, 28–38. [CrossRef]
135. Adánez-Rubio, I.; Abad, A.; Gayán, P.; Luis, F.; Adánez, J. CLOU process performance with a Cu-Mn oxygen carrier in the combustion of different types of coal with CO_2 capture. *Fuel* **2018**, *212*, 605–612. [CrossRef]
136. Li, J.; Li, J.; Zhu, Q.; Peng, W.; Li, H. Fabrication of hierarchical Co/MgO catalyst for enhanced CO_2 reforming of CH_4 in a fluidized-bed reactor. *AIChE J.* **2019**, *65*, 120–131. [CrossRef]
137. Moldenhauer, P.; Hallberg, P.; Biermann, M.; Snijkers, F.; Albertsen, K.; Mattisson, T.; Lyngfelt, A. Oxygen carrier development of calcium manganite-based materials with perovskite structure for chemical looping combustion of methane. In Proceedings of the 42nd International Technical Conference on Clean Energy, Clearwater, FL, USA, 11–15 June 2017.
138. Zhu, Y.; Liu, R.; Sun, X.; Ma, X.; Wang, X.; Tian, H. Metal modified hexaaluminates for syngas generation and CO_2 utilization via chemical looping. *Int. J. Hydrogen Energy* **2019**, *44*, 10218–10231. [CrossRef]

139. Huang, F.; Tian, M.; Zhu, Y.; Wang, X.; Wang, A.; Li, L.; Lin, J.; Wang, J. Fe-substituted Ba-hexaaluminate with enhanced oxygen mobility for CO_2 capture by chemical looping combustion of methane. *J. Energy Chem.* **2019**, *29*, 50–57. [CrossRef]
140. Pecchi, G.; Escalona, N.; Ghampson, I.T.; Morales, R. Energy production, decontamination, and hydrogenation reactions over perovskite-type oxide catalyst. In *Perovskite Materials—Synthesis, Characterisation, Properties, and Applications*; Pan, L., Zhu, G., Eds.; IntechOpen: London, UK, 2016.
141. Santinacci, L. ALD for photoelectrochemical water splitting. In *Atomic Layer Deposition in Energy Conversion Applications*; Bachmann, J., Ed.; Wiley-VCH Verlag GmbH & Co. KGaA: Weinheim, Germany, 2016.
142. Radha, R.; Sakar, M.; Bharathkumar, S.; Balakumar, S. Sunlight driven photocatalytic water splitting using nanostructured bismuth tungstate (Bi_2WO_6). *AIP Conf. Proc.* **2017**, *1832*, 050031.
143. Sathre, R.; Greenblatt, J.B.; Walczak, K.; Sharp, I.D.; Stevens, J.C.; Ager, J.W.; Houle, F.A. Opportunities to improve the net energy performance of photoelectrochemical water-splitting technology. *Energy Environ. Sci.* **2016**, *9*, 803–819. [CrossRef]
144. Sivula, K.; Van De Krol, R. Semiconducting materials for photoelectrochemical energy conversion. *Nat. Rev. Mater.* **2016**, *1*, 15010. [CrossRef]
145. Takata, T.; Domen, K. Development of non-oxide semiconductors as light harvesting materials in photocatalytic and photoelectrochemical water splitting. *Dalton Trans.* **2017**, *46*, 10529–10544. [CrossRef]
146. Smith, W.A. Photoelectrochemical cell design, efficiency, definitions, standards, and protocols. In *Photoelectrochemical Solar Fuel Production*; Giménez, S., Bisquert, J., Eds.; Springer: New York, NY, USA, 2016; pp. 163–197.
147. Sadeghi, N.; Sharifnia, S.; Arabi, M.S. A porphyrin-based metal organic framework for high rate photoreduction of CO_2 to CH_4 in gas phase. *J. CO_2 Util.* **2016**, *16*, 450–457. [CrossRef]
148. Tuller, H.L. Solar to fuels conversion technologies: A perspective. *Mater. Renew. Sustain. Energy* **2017**, *6*, 3. [CrossRef]
149. Toniolo, F.S.; Schmal, M. Improvement of catalytic performance of perovskites by partial substitution of cations and supporting on high surface area materials. In *Perovskite Materials—Synthesis, Characterisation, Properties, and Applications*; Pan, L., Zhu, G., Eds.; IntechOpen: London, UK, 2016.
150. Tobías, I.; Luque, A. Emerging high efficiency concepts for concentrator solar cells. In *Handbook of Concentrator Photovoltaic Technology*; Algora, C., Rey-Stolle, I., Eds.; John Wiley & Sons Ltd.: Hoboken, NY, USA, 2016; p. 137.
151. Block, T.; Knoblauch, N.; Schmücker, M. The cobalt-oxide/iron-oxide binary system for use as high temperature thermochemical energy storage material. *Thermochim. Acta* **2014**, *577*, 25–32. [CrossRef]
152. Takata, T.; Hisatomi, T.; Domen, K. Solar hydrogen production on some water splitting photocatalysts. In Proceedings of the Solar Hydrogen and Nanotechnology XI, San Diego, CA, USA, 28 August–1 September 2016; International Society for Optics and Photonics: Washington, DC, USA; p. 99350O.
153. Ussiri, D.A.; Lal, R. The role of bioenergy in mitigating climate change. In *Carbon Sequestration for Climate Change Mitigation and Adaptation*; Springer: New York, NY, USA, 2017; pp. 433–495.
154. Yang, W.; Moon, J. Recent advances in earth-abundant photocathodes for photoelectrochemical water splitting. *ChemSusChem* **2018**, *12*. [CrossRef] [PubMed]
155. Yan, F.; Zhu, C.; Li, C.; Zhang, S.; Zhang, X.; Chen, Y. Highly stable three-dimensional nickel–iron oxyhydroxide catalysts for oxygen evolution reaction at high current densities. *Electrochim. Acta* **2017**, *245*, 770–779. [CrossRef]
156. Vermaas, D.A.; Smith, W.A. Applications of bipolar membranes for electrochemical and photoelectrochemical water splitting. In *Advances in Photoelectrochemical Water Splitting: Theory, Experiment and Systems Analysis*; Tilley, S.D., Lany, S., van de Krol, R., Eds.; Royal Society of Chemistry: London, UK, 2018; pp. 208–238.
157. Waldie, K.M.; Kim, S.K.; Ingram, A.J.; Waymouth, R.M. Cyclopentadienyl cobalt complexes as precatalysts for electrocatalytic hydrogen evolution. *Eur. J. Inorg. Chem.* **2017**, *2017*, 2755–2761. [CrossRef]
158. Wu, P.; Liu, Z.; Chen, D.; Zhou, M.; Wei, J. Flake-like NiO/WO_3 pn heterojunction photocathode for photoelectrochemical water splitting. *Appl. Surf. Sci.* **2018**, *440*, 1101–1106. [CrossRef]
159. Zhang, Y.; Knibbe, R.; Sunarso, J.; Zhong, Y.; Zhou, W.; Shao, Z.; Zhu, Z. Solid-oxide fuel cells: Recent progress on advanced materials for solid-oxide fuel cells operating below 500 °C. *Adv. Mater.* **2017**, *29*, 1770345. [CrossRef]
160. Meda, L.; Abbondanza, L. Materials for photo-electrochemical water splitting. *Rev. Adv. Sci. Eng.* **2013**, *2*, 200–207. [CrossRef]

161. Schreier, M.; Curvat, L.; Giordano, F.; Steier, L.; Abate, A.; Zakeeruddin, S.M.; Luo, J.; Mayer, M.T.; Grätzel, M. Efficient photosynthesis of carbon monoxide from CO_2 using perovskite photovoltaics. *Nat. Commun.* **2015**, *6*, 7326. [CrossRef]
162. Jang, Y.J.; Jeong, I.; Lee, J.; Lee, J.; Ko, M.J.; Lee, J.S. Unbiased sunlight-driven artificial photosynthesis of carbon monoxide from CO_2 using a ZnTe-based photocathode and a perovskite solar cell in tandem. *ACS Nano* **2016**, *10*, 6980–6987. [CrossRef]
163. Kalamaras, E.; Maroto-Valer, M.M.; Shao, M.; Xuan, J.; Wang, H. Solar carbon fuel via photoelectrochemistry. *Catal. Today* **2018**, *317*, 56–75. [CrossRef]
164. Marquez, O.; Márquez, J. Synthesis of electrocatalysts for electrochemistry in energy. In *Advanced Solid Catalysts for Renewable Energy Production*; IGI Global: Hershey, PA, USA, 2018; pp. 300–385.
165. Marchi, M.; Niccolucci, V.; Pulselli, R.M.; Marchettini, N. Environmental policies for GHG emissions reduction and energy transition in the medieval historic centre of Siena (Italy): The role of solar energy. *J. Clean. Prod.* **2018**, *185*, 829–840. [CrossRef]
166. Li, F.; Bashir, S.; Liu, J.L. *Nanostructured Materials for Next-Generation Energy Storage and Conversion: Fuel Cells*; Springer: Berlin/Heidelberg, Germany, 2018.
167. Ning, X.; Li, W.; Meng, Y.; Qin, D.; Chen, J.; Mao, X.; Xue, Z.; Shan, D.; Devaramani, S.; Lu, X. New insight into procedure of interface electron transfer through cascade system with enhanced photocatalytic activity. *Small* **2018**, *14*, 1703989. [CrossRef] [PubMed]
168. Viswanathan, B. *Energy Sources: Fundamentals of Chemical Conversion Processes and Applications*; Elsevier: Amsterdam, The Netherlands, 2016.
169. Sugiyama, M.; Fujii, K.; Nakamura, S. Solar to chemical energy conversion. In *Lecture Notes Energy*; Springer: Basel, Switzerland, 2016; Volume 32, p. 253.
170. Thorpe, D.; Martin, C.L.; Goswami, D.Y. *Solar Energy Pocket Reference*; Routledge: London, UK, 2017.
171. Lari, M.O.; Sahin, A.Z. Design, performance and economic analysis of a nanofluid-based photovoltaic/thermal system for residential applications. *Energy Convers. Manag.* **2017**, *149*, 467–484. [CrossRef]
172. May, M.M.; Lewerenz, H.-J.; Lackner, D.; Dimroth, F.; Hannappel, T. Efficient direct solar-to-hydrogen conversion by in situ interface transformation of a tandem structure. *Nat. Commun.* **2015**, *6*, 8286. [CrossRef] [PubMed]
173. Yu, Z.; Sun, L. Inorganic hole-transporting materials for perovskite solar cells. *Small Methods* **2018**, *2*, 1700280. [CrossRef]
174. Reinders, A.; Verlinden, P.; Van Sark, W.; Freundlich, A. *Photovoltaic Solar Energy: From Fundamentals to Applications*; Reinders, A., Verlinden, P., van Sark, W., Freundlich, A., Eds.; John Wiley & Sons, Inc.: Hoboken, NY, USA, 2017.
175. Yu, Y.; Gao, P. Development of electron and hole selective contact materials for perovskite solar cells. *Chin. Chem. Lett.* **2017**, *28*, 1144–1152. [CrossRef]
176. Li, Q.; Zhang, P.; Yao, L.; Deng, L.; Ren, X.; Li, Y. Recent research progress on lead-free or less-lead perovskite solar cells. *Int. J. Electrochem. Sci.* **2017**, *12*, 4915–4927. [CrossRef]
177. Severance, C.A. A practical, affordable (and least business risk) plan to achieve "80% clean electricity" by 2035. *Electr. J.* **2011**, *24*, 8–26. [CrossRef]
178. Hagerman, G.; Polagye, B.; Bedard, R.; Previsic, M. *Methodology for Estimating Tidal Current Energy Resources and Power Production by Tidal In-Stream Energy Conversion (TISEC) Devices*; Technical Report No. EPRI–TP–001 NA Rev 2; EPRI: Palo Alto, CA, USA, 2006.
179. Li, R. Latest progress in hydrogen production from solar water splitting via photocatalysis, photoelectrochemical, and photovoltaic-photoelectrochemical solutions. *Chin. J. Catal.* **2017**, *38*, 5–12. [CrossRef]
180. Du, H.; Liu, Y.-N.; Shen, C.-C.; Xu, A.-W. Nanoheterostructured photocatalysts for improving photocatalytic hydrogen production. *Chin. J. Catal.* **2017**, *38*, 1295–1306. [CrossRef]
181. Lewis, N.S.; Nocera, D.G. Powering the planet: Chemical challenges in solar energy utilization. *Proc. Natl. Acad. Sci. USA* **2006**, *103*, 15729–15735. [CrossRef] [PubMed]
182. Solangi, K.; Islam, M.; Saidur, R.; Rahim, N.; Fayaz, H. A review on global solar energy policy. *Renew. Sustain. Energy Rev.* **2011**, *15*, 2149–2163. [CrossRef]
183. Timilsina, G.R.; Kurdgelashvili, L.; Narbel, P.A. Solar energy: Markets, economics and policies. *Renew. Sustain. Energy Rev.* **2012**, *16*, 449–465. [CrossRef]

184. Aman, M.; Solangi, K.; Hossain, M.; Badarudin, A.; Jasmon, G.; Mokhlis, H.; Bakar, A.; Kazi, S.N. A review of Safety, Health and Environmental (SHE) issues of solar energy system. *Renew. Sustain. Energy Rev.* **2015**, *41*, 1190–1204. [CrossRef]
185. Miller, E.L. Solar hydrogen production by photoelectrochemical water splitting: The promise and challenge. In *On Solar Hydrogen and Nanotechnology*; John Wiley & Sons (Asia) Pte. Ltd.: Singapore, 2009; pp. 3–35.
186. Zhu, W.H.; Zhu, Y.; Davis, Z.; Tatarchuk, B.J. Energy efficiency and capacity retention of Ni–MH batteries for storage applications. *Appl. Energy* **2013**, *106*, 307–313. [CrossRef]
187. Hoffmann, P. *Tomorrow's Energy: Hydrogen, Fuel Cells, and the Prospects for a Cleaner Planet*; MIT Press: Cambridge, MA, USA, 2012.
188. Herron, J.A.; Kim, J.; Upadhye, A.A.; Huber, G.W.; Maravelias, C.T. A general framework for the assessment of solar fuel technologies. *Energy Environ. Sci.* **2015**, *8*, 126–157. [CrossRef]
189. Fernández, J.; Abanades, J.; Murillo, R.; Grasa, G. Conceptual design of a hydrogen production process from natural gas with CO_2 capture using a Ca–Cu chemical loop. *Int. J. Greenh. Gas Control* **2012**, *6*, 126–141. [CrossRef]
190. Rostrup-Nielsen, J.R.; Sehested, J.; Nørskov, J.K. Hydrogen and synthesis gas by steam-and CO_2 reforming. *Adv. Catal.* **2002**, *47*, 65–139. [CrossRef]
191. Palzer, A.; Henning, H.M. A future German energy system with a dominating contribution from renewable energies: A holistic model based on hourly simulation. *Energy Technol.* **2014**, *2*, 13–28. [CrossRef]
192. Palzer, A.; Henning, H.-M. A comprehensive model for the German electricity and heat sector in a future energy system with a dominant contribution from renewable energy technologies—Part II: Results. *Renew. Sustain. Energy Rev.* **2014**, *30*, 1019–1034. [CrossRef]
193. Murugadoss, G.; Thangamuthu, R.; Kumar, S.M.S. Fabrication of $CH_3NH_3PbI_3$ perovskite-based solar cells: Developing various new solvents for CuSCN hole transport material. *Sol. Energy Mater. Sol. Cells* **2017**, *164*, 56–62. [CrossRef]
194. Nair, M.M.; Abanades, S.P. Tailoring hybrid nonstoichiometric ceria redox cycle for combined solar methane reforming and thermochemical conversion of H_2O/CO_2. *Energy Fuels* **2016**, *30*, 6050–6058. [CrossRef]
195. Montoya, J.H.; Seitz, L.C.; Chakthranont, P.; Vojvodic, A.; Jaramillo, T.F.; Nørskov, J.K. Materials for solar fuels and chemicals. *Nat. Mater.* **2017**, *16*, 70. [CrossRef]
196. Ohsato, H. Microwave dielectrics with perovskite-type structure. In *Perovskite Materials—Synthesis, Characterisation, Properties, and Applications*; Pan, L., Zhu, G., Eds.; IntechOpen: London, UK, 2016.
197. Yamazaki, Y. Solar-Driven Thermochemical CO_2 Reduction Using Nonstoichiometric Perovskite. 2016. Available online: https://dc.engconfintl.org/nonstoichiometric_vi/15 (accessed on 9 January 2020).
198. Demont, A.; Abanades, S. Solar thermochemical conversion of CO_2 into fuel via two-step redox cycling of non-stoichiometric Mn-containing perovskite oxides. *J. Mater. Chem. A* **2015**, *3*, 3536–3546. [CrossRef]
199. Nair, M.M.; Abanades, S. Experimental screening of perovskite oxides as efficient redox materials for solar thermochemical CO_2 conversion. *Sustain. Energy Fuels* **2018**, *2*, 843–854. [CrossRef]
200. Dey, S.; Rao, C. Splitting of CO_2 by manganite perovskites to generate CO by solar isothermal redox cycling. *ACS Energy Lett.* **2016**, *1*, 237–243. [CrossRef]
201. Nair, M.M.; Abanades, S. Insights into the redox performance of non–stoichiometric lanthanum manganite perovskites for solar thermochemical CO_2 splitting. *ChemistrySelect* **2016**, *1*, 4449–4457. [CrossRef]
202. Riaz, A.; Kreider, P.; Kremer, F.; Tabassum, H.; Yeoh, J.S.; Lipiński, W.; Lowe, A. Electrospun manganese-based perovskites as efficient oxygen exchange redox materials for improved solar thermochemical CO_2 splitting. *ACS Appl. Energy Mater.* **2019**, *2*, 2494–2505. [CrossRef]
203. Carrillo, A.J.; Bork, A.H.; Moser, T.; Sediva, E.; Hood, Z.D.; Rupp, J.L. Modifying $La_{0.6}Sr_{0.4}MnO_3$ perovskites with Cr incorporation for fast isothermal CO_2-splitting kinetics in solar-driven thermochemical cycles. *Adv. Energy Mater.* **2019**, *9*, 1803886. [CrossRef]
204. Bork, A.H.; Povoden-Karadeniz, E.; Carrillo, A.J.; Rupp, J.L. Thermodynamic assessment of the solar-to-fuel performance of $La_{0.6}Sr_{0.4}Mn_{1-Y}Cr_yO_3$ perovskite solid solution series. *Acta Mater.* **2018**, *178*, 163–172. [CrossRef]
205. Luciani, G.; Landi, G.; Aronne, A.; Di Benedetto, A. Partial substitution of B cation in $La_{0.6}Sr_{0.4}MnO_3$ perovskites: A promising strategy to improve the redox properties useful for solar thermochemical water and carbon dioxide splitting. *Sol. Energy* **2018**, *171*, 1–7. [CrossRef]

206. Ezbiri, M.; Becattini, V.; Hoes, M.; Michalsky, R.; Steinfeld, A. High redox capacity of Al-doped $La_{1-x}Sr_xMnO_{3-\delta}$ perovskites for splitting CO_2 and H_2O at Mn-enriched surfaces. *ChemSusChem* **2017**, *10*, 1517–1525. [CrossRef] [PubMed]
207. Cooper, T.; Scheffe, J.R.; Galvez, M.E.; Jacot, R.; Patzke, G.; Steinfeld, A. Lanthanum manganite perovskites with Ca/Sr A-site and Al B-site doping as effective oxygen exchange materials for solar thermochemical fuel production. *Energy Technol.* **2015**, *3*, 1130–1142. [CrossRef]
208. Sastre, D.; Carrillo, A.; Serrano, D.; Pizarro, P.; Coronado, J. Exploring the redox behavior of LaSrMnAlO perovskites for CO-splitting in thermochemical cycles. *Top. Catal.* **2017**, *60*, 1108–1118. [CrossRef]
209. Bork, A.H.; Kubicek, M.; Struzik, M.; Rupp, J.L. Perovskite $La_{0.6}Sr_{0.4}Cr_{1-x}$ $Co_xO_{3-\delta}$ solid solutions for solar-thermochemical fuel production: Strategies to lower the operation temperature. *J. Mater. Chem. A* **2015**, *3*, 15546–15557. [CrossRef]
210. Hare, B.J.; Maiti, D.; Daza, Y.A.; Bhethanabotla, V.R.; Kuhn, J.N. Enhanced CO_2 conversion to CO by silica-supported perovskite oxides at low temperatures. *ACS Catal.* **2018**, *8*, 3021–3029. [CrossRef]
211. Hare, B.J.; Maiti, D.; Ramani, S.; Ramos, A.E.; Bhethanabotla, V.R.; Kuhn, J.N. Thermochemical conversion of carbon dioxide by reverse water-gas shift chemical looping using supported perovskite oxides. *Catal. Today* **2019**, *323*, 225–232. [CrossRef]
212. Hare, B.J.; Maiti, D.; Meier, A.; Bhethanabotla, V.R.; Kuhn, J.N. CO_2 conversion performance of perovskite oxides designed with abundant metals. *Ind. Eng. Chem. Res.* **2019**, *58*, 12551–12560. [CrossRef]
213. Ramos, A.E.; Maiti, D.; Daza, Y.A.; Kuhn, J.N.; Bhethanabotla, V.R. Co, Fe, and Mn in La-perovskite oxides for low temperature thermochemical CO_2 conversion. *Catal. Today* **2019**, *338*, 52–59. [CrossRef]
214. Dey, S.; Naidu, B.; Rao, C. $Ln_{0.5}A_{0.5}MnO_3$ (Ln = Lanthanide, A = Ca, Sr) perovskites exhibiting remarkable performance in the thermochemical generation of CO and H_2 from CO_2 and H_2O. *Chem. A Eur. J.* **2015**, *21*, 7077–7081. [CrossRef] [PubMed]
215. Rao, C.; Dey, S. Generation of H_2 and CO by solar thermochemical splitting of H_2O and CO_2 by employing metal oxides. *J. Solid State Chem.* **2016**, *242*, 107–115. [CrossRef]
216. Takalkar, G.; Bhosale, R.R. Solar thermocatalytic conversion of CO_2 using $Pr_xSr_{(1-x)}MnO_{3-\delta}$ perovskites. *Fuel* **2019**, *254*, 115624. [CrossRef]
217. Takalkar, G.; Bhosale, R.; AlMomani, F. Combustion synthesized $A_{0.5}Sr_{0.5}MnO_{3-\delta}$ perovskites (where, a = La, Nd, Sm, Gd, Tb, Pr, Dy, and Y) as redox materials for thermochemical splitting of CO_2. *Appl. Surf. Sci.* **2019**. [CrossRef]
218. Mulmi, S.; Chen, H.; Hassan, A.; Marco, J.F.; Berry, F.J.; Sharif, F.; Slater, P.R.; Roberts, E.P.; Adams, S.; Thangadurai, V. Thermochemical CO_2 splitting using double perovskite-type $Ba_2Ca_{0.66}Nb_{1.34-x}Fe_xO_{6-\delta}$. *J. Mater. Chem. A* **2017**, *5*, 6874–6883. [CrossRef]
219. Zhang, J.; Haribal, V.; Li, F. Perovskite nanocomposites as effective CO_2-splitting agents in a cyclic redox scheme. *Sci. Adv.* **2017**, *3*, e1701184. [CrossRef]
220. Xu, Y.-F.; Yang, M.-Z.; Chen, B.-X.; Wang, X.-D.; Chen, H.-Y.; Kuang, D.-B.; Su, C.-Y. A $CsPbBr_3$ perovskite quantum dot/graphene oxide composite for photocatalytic CO_2 reduction. *J. Am. Chem. Soc.* **2017**, *139*, 5660–5663. [CrossRef]
221. Hou, J.; Cao, S.; Wu, Y.; Gao, Z.; Liang, F.; Sun, Y.; Lin, Z.; Sun, L. Inorganic colloidal perovskite quantum dots for robust solar CO_2 reduction. *Chem. Eur. J.* **2017**, *23*, 9481–9485. [CrossRef]
222. Guo, S.-H.; Zhou, J.; Zhao, X.; Sun, C.-Y.; You, S.-Q.; Wang, X.-L.; Su, Z.-M. Enhanced CO_2 photoreduction via tuning halides in perovskites. *J. Catal.* **2019**, *369*, 201–208. [CrossRef]
223. Zhou, L.; Xu, Y.F.; Chen, B.X.; Kuang, D.B.; Su, C.Y. Synthesis and photocatalytic application of stable lead-free $Cs_2AgBiBr_6$ perovskite nanocrystals. *Small* **2018**, *14*, 1703762. [CrossRef]
224. Xu, Y.-F.; Yang, M.-Z.; Chen, H.-Y.; Liao, J.-F.; Wang, X.-D.; Kuang, D.-B. Enhanced solar-driven gaseous CO_2 conversion by $CsPbBr_3$ nanocrystal/Pd nanosheet Schottky-junction photocatalyst. *ACS Appl. Energy Mater.* **2018**, *1*, 5083–5089. [CrossRef]
225. Wan, S.; Ou, M.; Zhong, Q.; Wang, X. Perovskite-type $CsPbBr_3$ quantum dots/UiO-66 (NH_2) nanojunction as efficient visible-light-driven photocatalyst for CO_2 reduction. *Chem. Eng. J.* **2019**, *358*, 1287–1295. [CrossRef]
226. Wang, B.; Di, J.; Lu, L.; Yan, S.; Liu, G.; Ye, Y.; Li, H.; Zhu, W.; Li, H.; Xia, J. Sacrificing ionic liquid-assisted anchoring of carbonized polymer dots on perovskite-like $PbBiO_2Br$ for robust CO_2 photoreduction. *Appl. Catal. B Environ.* **2019**, *254*, 551–559. [CrossRef]

227. Shan, J.; Raziq, F.; Humayun, M.; Zhou, W.; Qu, Y.; Wang, G.; Li, Y. Improved charge separation and surface activation via boron-doped layered polyhedron $SrTiO_3$ for co-catalyst free photocatalytic CO_2 conversion. *Appl. Catal. B Environ.* **2017**, *219*, 10–17. [CrossRef]
228. Wang, Y.; Liu, M.; Chen, W.; Mao, L.; Shangguan, W. Ag loaded on layered perovskite $H_2SrTa_2O_7$ to enhance the selectivity of photocatalytic CO_2 reduction with H_2O. *J. Alloys Compd.* **2019**, *786*, 149–154. [CrossRef]
229. Hafez, A.M.; Zedan, A.F.; AlQaradawi, S.Y.; Salem, N.M.; Allam, N.K. Computational study on oxynitride perovskites for CO_2 photoreduction. *Energy Convers. Manag.* **2016**, *122*, 207–214. [CrossRef]
230. Hou, J.; Cao, S.; Wu, Y.; Liang, F.; Ye, L.; Lin, Z.; Sun, L. Perovskite-based nanocubes with simultaneously improved visible-light absorption and charge separation enabling efficient photocatalytic CO_2 reduction. *Nano Energy* **2016**, *30*, 59–68. [CrossRef]
231. Wang, Q.; Tao, L.; Jiang, X.; Wang, M.; Shen, Y. Graphene oxide wrapped $CH_3NH_3PbBr_3$ perovskite quantum dots hybrid for photoelectrochemical CO_2 reduction in organic solvents. *Appl. Surf. Sci.* **2019**, *465*, 607–613. [CrossRef]
232. Yu, J.; Cheng, G.; Luo, W. 3D mesoporous rose-like nickel-iron selenide microspheres as advanced electrocatalysts for the oxygen evolution reaction. *Nano Res.* **2018**, *11*, 2149–2158. [CrossRef]
233. Pilatos, G.; Perdikaki, A.V.; Sapalidis, A.; Pappas, G.S.; Giannakopoulou, T.; Tsoutsou, D.; Xenogiannopoulou, E.; Boukos, N.; Dimoulas, A.; Trapalis, C. Graphene by one-step chemical vapor deposition from ferrocene vapors: Properties and electrochemical evaluation. *J. Appl. Phys.* **2016**, *119*, 064303. [CrossRef]
234. Vermisoglou, E.C.; Karanikolos, G.N.; Pilatos, G.; Devlin, E.; Romanos, G.E.; Veziri, C.U.; Kanellopoulos, N.K. Aligned carbon nanotubes with ferromagnetic behavior. *Adv. Mater.* **2010**, *22*, 473–477. [CrossRef] [PubMed]